Article

Fibroblast growth factor receptor 3 in hepatocytes protects from toxin-induced liver injury and fibrosis

Chronic toxic injury

Fgfr3 expressed in hepatocytes

Liver fibrosis

Fgfr3 deleted in hepatocytes

Severe liver fibrosis

Hepatocyte   Stellate cell   Kupffer cell   Fgfr3

Damaged hepatocyte   Endothelial cell   Extracellular matrix   Fgf9/18

Figure created using BioRender.com

Abbie E. Fearon, Coenraad F. Slabber, Andrii Kuklin, ..., Lin Chen, Manfred Kopf, Sabine Werner

sabine.werner@biol.ethz.ch

Highlights

Fgfr3 is important for hepatocyte survival following CCl$_4$-induced liver injury

Fgfr3 in hepatocytes regulates expression of metabolic and pro-fibrotic genes

Fgfr3 protects from extensive fibrosis after chronic CCl$_4$ treatment

Fgf receptors have unique, but also overlapping functions in hepatocytes
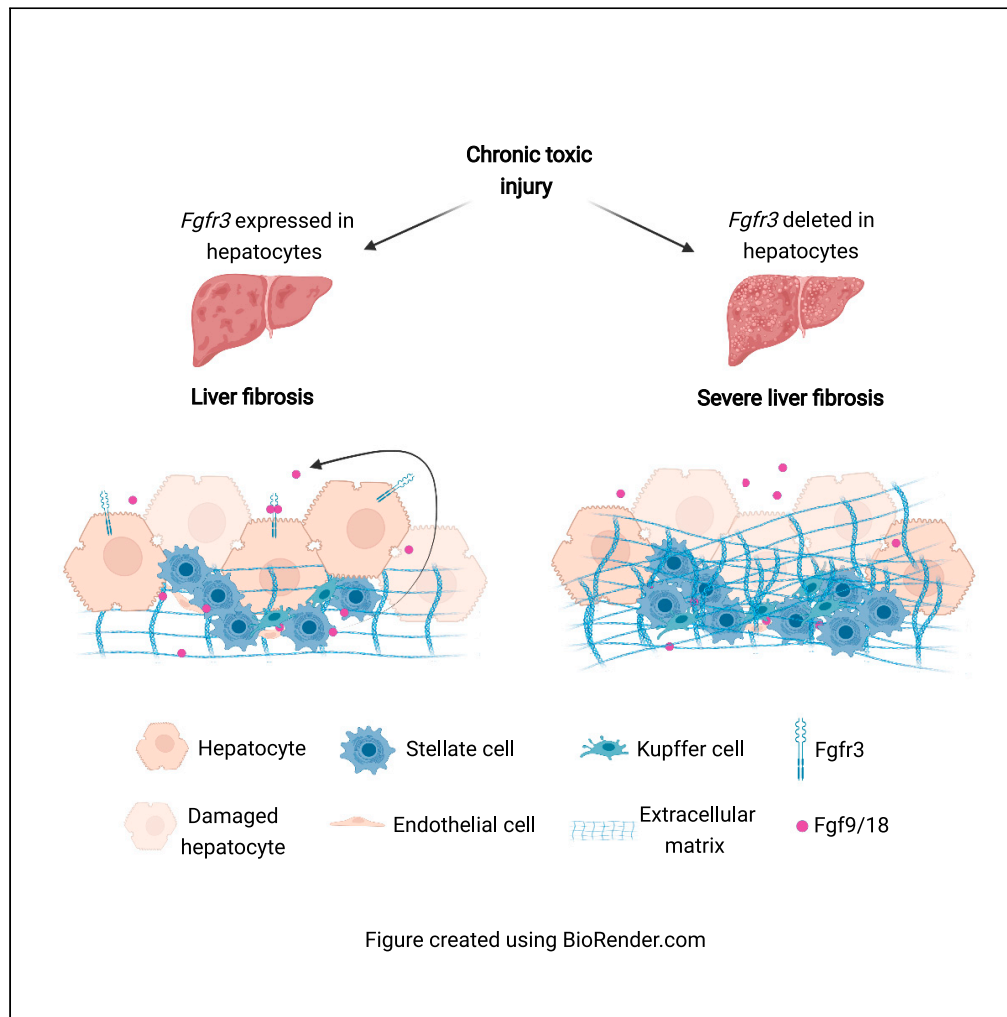
iScience

Article

Fibroblast growth factor receptor 3 in hepatocytes protects from toxin-induced liver injury and fibrosis

Abbie E. Fearon,[1,4] Coenraad F. Slabber,[1,4] Andrii Kuklin,[1] Marc Bachofner,[1] Luigi Tortola,[1] Lea Pohlmeier,[1] Sophia Pantasis,[1] Thorsten Hornemann,[2] Lin Chen,[3] Manfred Kopf,[1] and Sabine Werner[1,5,*]

SUMMARY

The liver's remarkable regenerative capacity is orchestrated by several growth factors and cytokines. Fibroblast growth factor receptor 3 (Fgfr3) is frequently overexpressed in hepatocellular carcinoma and promotes cancer aggressiveness, whereas its role in liver homeostasis, repair and regeneration is unknown. We show here that Fgfr3 is expressed by hepatocytes in the healthy liver. Its major ligand, Fgf9, is mainly expressed by non-parenchymal cells and upregulated upon injury. Mice lacking Fgfr3 in hepatocytes exhibit increased tissue necrosis after acute toxin treatment and more excessive fibrosis after long-term injury. This was not a consequence of immunological alterations in the non-injured liver as revealed by comprehensive flow cytometry analysis. Rather, loss of Fgfr3 altered the expression of metabolic and pro-fibrotic genes in hepatocytes. These results identify a paracrine Fgf9-Fgfr3 signaling pathway that protects from toxin-induced cell death and the resulting liver fibrosis and suggests a potential use of FGFR3 ligands for therapeutic purposes.

INTRODUCTION

The liver fulfills many essential metabolic functions and is also the major detoxifying organ of the body. Therefore, any insult to the liver has to be rapidly and efficiently repaired. In contrast to other organs of adult mammals, which heal with scar formation, the liver has the unique capability to fully regenerate (Diehl, 2002; Michalopoulos, 2007). This occurs by hyperproliferation of the remaining differentiated liver cells and/or by activation of pluripotent precursor cells, depending on the type and extent of injury (Michalopoulos, 2007; Williams et al., 2014). However, when the remaining tissue is too small, the organ is in a critical state and liver failure is frequent (Serenari et al., 2013). In addition, chronic liver injury impairs the ability to regenerate. In this case, prolonged inflammation occurs, and liver fibrosis and cirrhosis may develop. This is a frequent consequence of chronic viral hepatitis or drug and/or alcohol abuse (Lee et al., 2015; Trautwein et al., 2015). Although the prevalence of such conditions is high worldwide, therapeutic approaches are still unsatisfactory. Therefore, a thorough understanding of the mechanisms underlying liver homeostasis and regeneration, as well as identification of the factors that orchestrate this process, is of key relevance.

A plethora of growth factors and cytokines are expressed in the regenerating liver and/or the adjacent spleen. Ligands of the epidermal growth factor receptor (EGFR) as well as hepatocyte growth factor (HGF) are major hepatocyte mitogens with crucial functions in liver regeneration and fibrosis (Böhm et al., 2010a). More recently, important functions of fibroblast growth factors (FGFs) in the regeneration process of this organ have been discovered (Maddaluno et al., 2017; Seitz and Hellerbrand, 2021). FGFs comprise a family of 22 proteins in mammals, and most of them signal by activation of four transmembrane tyrosine kinase receptors, designated FGFR1 – FGFR4 (Ornitz and Itoh, 2015). We previously showed that murine liver regeneration after partial hepatectomy (PH) is severely impaired upon combined loss of Fgfr1 and Fgfr2 in hepatocytes (Böhm et al., 2010b). In addition, siRNA-mediated knock-down of Fgfr4 in hepatocytes or global knockout of the major Fgfr4 ligand, Fgf15, strongly impaired the regeneration process in the same injury model (Padrissa-Altés et al., 2015; Kong et al., 2014; Uriarte et al., 2013). Finally, siRNA-mediated knock-down of Fgfr4 in hepatocytes of mice lacking Fgfr1 and Fgfr2 in these cells caused liver failure after PH (Padrissa-Altés et al., 2015), demonstrating an essential role of FGFR signaling in general for liver regeneration and some overlapping activities of the FGF receptors in hepatocytes. However,

[1]Institute of Molecular Health Sciences, Swiss Federal Institute of Technology (ETH) Zurich, Otto-Stern-Weg 7, 8093 Zurich, Switzerland

[2]Institute of Clinical Chemistry, University Hospital Zurich, 8092 Zurich, Switzerland

[3]Center of Bone Metabolism and Repair, Department of Rehabilitation Medicine, State Key Laboratory of Trauma, Burns and Combined Injury, Trauma Center, Institute of Surgery Research, Daping Hospital, Third Military Medical University, Chongqing 400042, China

[4]These authors have contributed equally

[5]Lead contact

*Correspondence:
sabine.werner@biol.ethz.ch

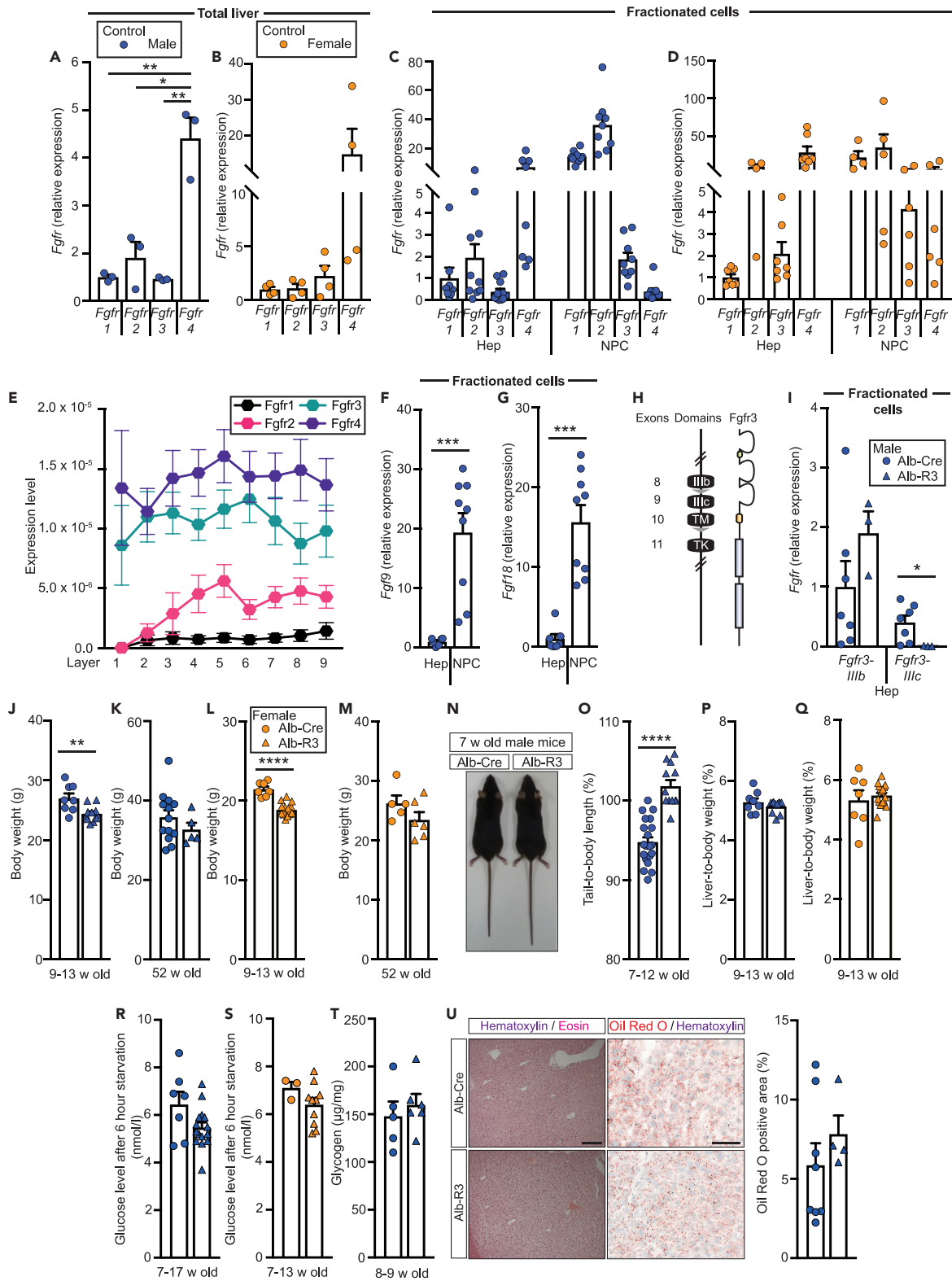https://doi.org/10.1016/j.isci.2021.103143

Figure 1. Fgfr3 is expressed in hepatocytes, but is dispensable for liver homeostasis

(A and B) qRT-PCR analysis of whole liver RNA from male (A, blue circles) or female (B, orange circles) wild-type mice for *Fgfr1*, *Fgfr2*, *Fgfr3* and *Fgfr4* relative to *Gapdh*. Expression levels of *Fgfr1* were set to 1.

Figure 1. *Continued*

(C and D) qRT-PCR analysis of RNA from isolated hepatocytes (Hep) and non-parenchymal cells (NPC) of male (C) or female (D) mice for *Fgfr1*, *Fgfr2*, *Fgfr3* and *Fgfr4* relative to *Gapdh*. Expression levels of *Fgfr1* in hepatocytes were set to 1.

(E) Zonal expression of *Fgfr1*, *Fgfr2*, *Fgfr3* and *Fgfr4* in liver from the central vein (layer 1) to the portal triad (layer 8) based on published data (Halpern et al., 2017).

(F and G) qRT-PCR analysis of RNA from Hep and NPC of male mice for *Fgf9* (F) and *Fgf18* (G). Mean expression levels of Fgf ligands in hepatocytes were set to 1.

(H) Schematic representation of the floxed *Fgfr3* allele and the Fgfr3 protein. In the *Fgfr3* conditional knockout allele, *loxP* sites (gray arrow heads) flank exons 9 and 10, encompassing the coding sequences for the IIIc and transmembrane (TM) domains (Su et al., 2010).

(I) qRT-PCR analysis of RNA from Hep of male Alb-Cre (blue circles) and Alb-R3 mice (blue triangles) for *Fgfr3* (IIIb and IIIc splice variants). Mean RNA levels of the Fgfr-IIIb variant in hepatocytes of Alb-Cre mice were set to 1.

(J–M) Body weight of 9-13- (J and L) and 52-week-old (K and M) male (J, K, blue) or female (L, M, orange) Alb-Cre (circles) and Alb-R3 (triangles) mice.

(N) Representative images of seven-week-old male Alb-Cre and Alb-R3 mice showing body and tail.

(O) Tail-to-body length ratio of 7-12-week-old male Alb-Cre and Alb-R3 mice.

(P and Q) Liver-to-body weight ratio of 9-13-week-old male (P) or female (Q) Alb-Cre and Alb-R3 mice.

(R and S) Blood glucose levels of 7-17-week-old male (R) and 7-13-week-old female (S) Alb-Cre and Alb-R3 mice 6 h after starvation.

(T) Liver glycogen content in 8-9-week-old male Alb-Cre and Alb-R3 mice at 10 a.m.

(U) Representative photomicrographs of hematoxylin/eosin- and Oil Red O/hematoxylin-stained liver sections from adult male mice. Magnification bars: 40 μm (left) and 100 μm (right). Oil Red O positive area was determined by analyzing 5 independent microscopic fields (20x magnification) per animal and is plotted as percentage of total liver area.

Bar graphs show mean ± SEM. N = 3 (A), N = 4 (B), N = 8–11 (C), N = 4–7 (D), N = 9 (E), N = 6–9 (F), N = 7–9 (G), N = 3–7 (I), N = 8–11 (J), N = 5–13 (K), N = 7–17 (L), N = 5–6 (M), N = 12–21 (O), N = 8–11 (P), N = 7–17 (Q), N = 7–15 (R), N = 3–10 (S), N = 5–6 (T) and N = 4–8 (U). *p ≤ 0.05, **p ≤ 0.01, ***p ≤ 0.001 and ****p ≤ 0.0001 (t test (A) or Mann-Whitney U test (F, G, I, J, L and O)).

some of the mice survived, indicating compensatory mechanisms, which may be mediated through Fgfr3, whose function in normal hepatocytes is so far unclear. This receptor is strongly expressed by human hepatoma cells *in vitro* and *in vivo* (Paur et al., 2015), and a major ligand of FGFR3, FGF9, was identified as a potent hepatocyte and hepatoma cell mitogen (Antoine et al., 2007; Paur et al., 2020; Seitz et al., 2020). Here, we show that loss of Fgfr3 in hepatocytes aggravates toxin-induced liver injury and fibrosis in mice. These and the previous findings obtained with other FGFR knockout mice identify unique and overlapping functions of FGF receptors in liver regeneration through regulation of common and distinct target genes.

RESULTS

Fgfr3 is expressed by different cell types of the liver

To study the function of Fgfr3 in the liver, we first analyzed its expression pattern by qRT-PCR. All FGF receptors were expressed in the liver of adult male and female mice, with *Fgfr4* being expressed at the highest level (Figures 1A and 1B). *Fgfr4* is mainly expressed by hepatocytes, whereas expression of the other FGF receptors is more pronounced in non-parenchymal cells (NPC). However, hepatocytes also express these receptors (Figures 1C and 1D). Published RNA-sequencing data (Halpern et al., 2017) further show that FGF receptors are expressed at similar levels in different zones of the liver lobules (Figure 1E). FGFR3 mRNA and protein were also detected in hepatocytes of normal human liver (see Human Protein Atlas https://www.proteinatlas.org/ENSG00000068078-FGFR3/tissue/liver#img). mRNA encoding two major ligands of Fgfr3, Fgf9, and Fgf18 (Zhang et al., 2006), were predominantly expressed by NPCs (Figures 1F and 1G), consistent with the previously demonstrated expression of FGF9 by hepatic stellate cells in human liver and in culture (Antoine et al., 2007; Paur et al., 2020; Seitz et al., 2020). These results suggest that NPC-derived FGFs activate Fgfr3 in hepatocytes in a paracrine manner.

Fgfr3 in hepatocytes is dispensable for liver homeostasis and regeneration after partial hepatectomy

To gain insight into the postnatal function of Fgfr3 in hepatocytes, we generated hepatocyte-specific *Fgfr3* knockout mice (Alb-R3 mice). The *Fgfr3* targeting strategy results in the deletion of exon IIIc and the transmembrane domain upon Cre-mediated recombination (Su et al., 2010) (Figure 1H). Therefore, a functional FGFR cannot be expressed in the targeted cells, but RNA that may potentially give rise to a truncated, nonfunctional protein including the IIIb domain of the receptor, can still be produced. mRNA encoding the IIIc exon was indeed no longer detectable in isolated hepatocytes of Alb-R3 mice, demonstrating the efficient knockout (Figure 1I). As expected, (truncated) transcripts that include the coding sequences for the IIIb exon of Fgfr3 were still present (Figure 1I).
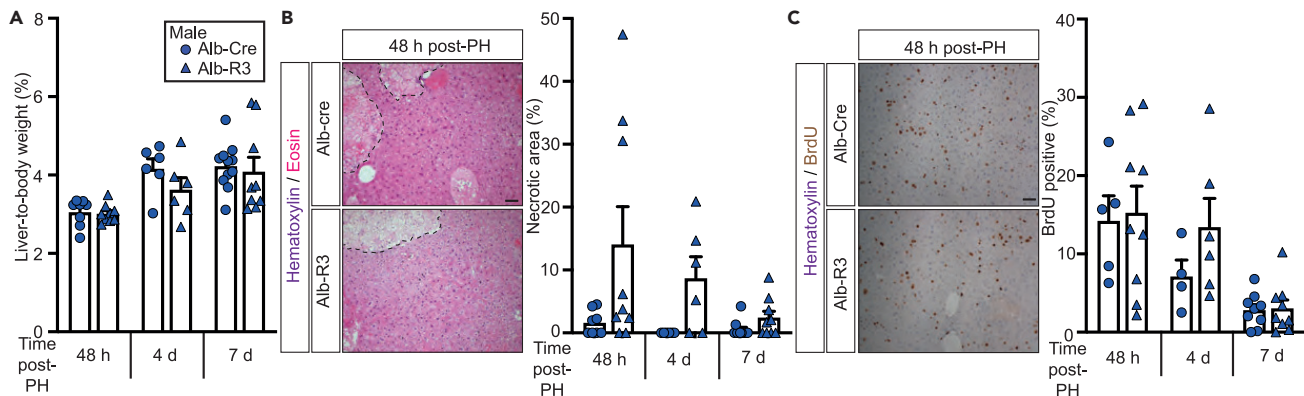
Figure 2. Fgfr3 is not essential for liver regeneration after PH

(A) Liver-to-body weight ratio of male mice at the indicated time points after PH.

(B) Representative photomicrographs of hematoxylin/eosin-stained liver sections of male mice 48 h after PH. Necrotic area is encircled with a black dotted line. Magnification bar: 50 μm. Graph shows quantification of necrotic areas at the indicated time points. Necrotic area was determined by analyzing 5 independent microscopic fields (20x magnification) per animal and is plotted as percentage of total liver area.

(C) Representative photomicrographs of BrdU-stained liver sections of male mice 48 h post PH, counterstained with hematoxylin. Scale bar: 50 μm. BrdU-positive hepatocytes (brown nuclei) were counted in 5 independent microscopic fields (20x magnification) per animal, and the percentage of BrdU-positive hepatocytes is shown in the graph.

Bar graphs show mean ± SEM. Circles indicate Alb-Cre mice and triangles indicate Alb-R3 mice. N = 6–11 (A, B) and N = 4–9 (C).

Alb-R3 mice were viable and fertile. Both male and female mice had a significantly reduced body weight at the age of 9-13-weeks, but this was no longer observed upon aging (Figures 1J−1M). Of note, they had a longer tail than control mice (Figures 1N and 1O). A similar, although more pronounced, phenotype has been described for mice with global *Fgfr3* knockout (Li et al., 1999). Because the albumin promoter is only active in hepatocytes (Postic et al., 1999), this finding suggests that the elongated tail phenotype not only results from *Fgfr3* deletion in the bone, but also from loss of this receptor in hepatocytes, which may lead to metabolic/systemic abnormalities. The *Fgfr3* knockout did not affect the liver-to-body weight ratio, blood glucose levels after 6 h starvation or glycogen content in the morning (Figures 1P−1T), and there were no histological signs of necrosis, inflammation, steatosis, or fibrosis under homeostatic conditions (Figure 1U).

We next subjected the mice to PH, where two-thirds of the liver is surgically removed. PH induces compensatory hyperproliferation of the remaining hepatocytes along with minimal necrosis or inflammation (Michalopoulos, 2007; Taub, 2004). Loss of Fgfr3 did not affect the liver-to-body weight ratio after PH (Figure 2A). Larger necrotic areas were seen in some Alb-R3 mice between 48 h and 7 d post-PH, but this was not consistently observed, and the difference was therefore not statistically significant (Figure 2B). There was no reduction in hepatocyte proliferation in Alb-R3 *vs* Alb-Cre mice (Figure 2C), but rather a mild increase at day 4 after PH, which may reflect the requirement to repair a more extensive damage.

Fgfr3 in hepatocytes is important for cell survival after toxin-induced liver injury

To further test a potential hepatoprotective function of Fgfr3, we induced liver damage by a single intraperitoneal injection of carbon tetrachloride (CCl_4), which induces necrosis and inflammation followed by repair of the injured tissue (Mehendale et al., 1994). Expression levels of Fgf9 increased in NPCs within 48 h of acute CCl_4 treatment, and highest levels in the liver were seen 5 d post-CCl_4 injection in mice of both genotypes (Figures 3A and 3B). Verification of hepatocyte and NPC purity was confirmed via protein tyrosine phosphatase receptor type C (*Ptprc*) and vimentin (*Vim*) expression (Figures 3C and 3D). The area of necrotic tissue was significantly increased in Alb-R3 *vs* Alb-Cre mice between 24 h and 5 d post CCl_4 injection (Figure 3E). As expected, a single vehicle (olive oil) injection did not cause liver injury (Figure 3E). The liver damage in CCl_4-treated mice was reflected by a mild, although non-significant increase in serum levels of AST and ALT at 24 h post CCl_4 injection between Alb-R3 and Alb-Cre mice (Figures 3F and 3G), whereas the liver-to-body weight ratio was not affected by the *Fgfr3* knockout (Figure 3H). CCl_4 treatment promoted proliferation of liver cells in mice of both genotypes; however, there was no significant difference between mice of both genotypes at any time point (Figures 3I and 3J). The more severe liver damage in
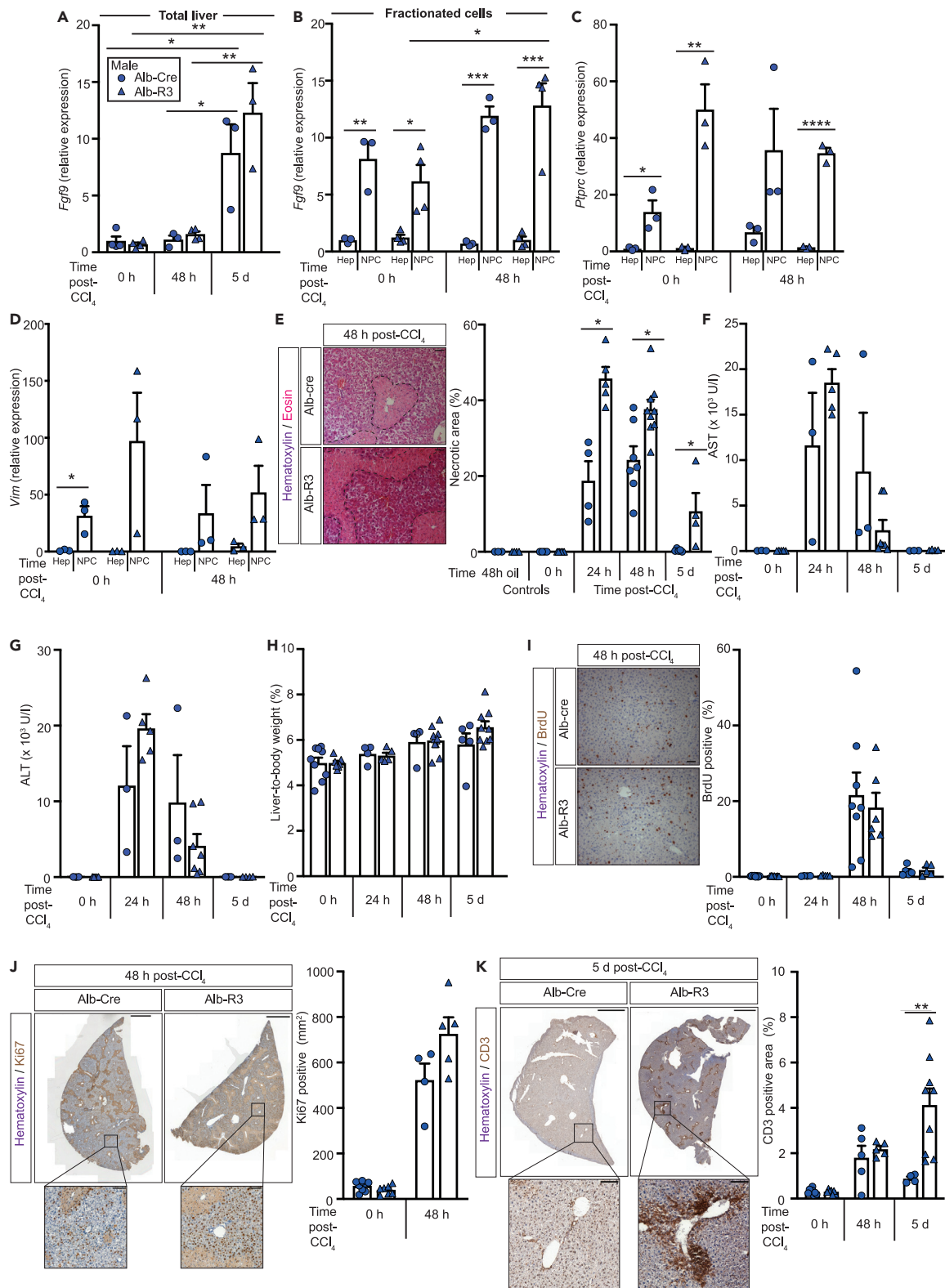
Figure 3. Loss of Fgfr3 in hepatocytes aggravates liver necrosis after acute CCl₄ injury

(A) qRT-PCR analysis of whole liver RNA from Alb-Cre and Alb-R3 mice at different time points after CCl₄ injection for *Fgf9*. Mean expression levels in untreated Alb-Cre mice (0 h) were set to 1.

Figure 3. *Continued*

(B) qRT-PCR analysis of RNA from isolated Hep and NPC of male Alb-Cre and Alb-R3 mice at 0 h and 48 h after CCl$_4$ injection for *Fgf9*. Mean expression levels in hepatocytes were set to 1.

(C and D) qRT-PCR analysis of RNA from Hep and NPCs of male Alb-Cre and Alb-R3 mice at 0 h or 48 h after CCl$_4$ injection for *Ptprc* and *Vim*. Expression levels in hepatocytes at 0 h were set to 1.

(E) Representative photomicrographs of hematoxylin/eosin-stained liver sections 48 h after acute CCl$_4$ injury from Alb-Cre and Alb-R3 mice. Magnification bar: 50 μm. Necrotic area (encircled) was determined by analyzing 5 independent microscopic fields (20x magnification) per mouse and is plotted as percentage of total liver area. Non-treated mice (0 h) or mice injected with the vehicle (oil) were used as controls.

(F and G) AST and ALT serum levels in control animals (0 h) and 24 h, 48 h and 5 d after CCl$_4$ injury in Alb-Cre and Alb-R3 mice.

(H) Liver-to-body weight ratio of male Alb-Cre and Alb-R3 mice at the indicated time points after a single CCl$_4$ injection.

(I) Representative photomicrographs of BrdU-stained liver sections from Alb-Cre and Alb-R3 mice 48 h after acute CCl$_4$ injury, counterstained with hematoxylin. Magnification bars: 50 μm. Graph shows the percentage of BrdU-positive hepatocytes among all hepatocytes. BrdU-positive hepatocytes (brown nuclei) were counted in 5 independent microscopic fields (20x magnification) per animal and the percentage of BrdU-positive hepatocytes is shown in the graph.

(J) Representative liver sections of Alb-Cre and Alb-R3 mice immuno-stained for Ki67 and counterstained with hematoxylin 48 h after CCl$_4$ injection. Graph shows number of Ki67-positive cells/mm^2 in one section per animal in 0 h and 48 h CCl$_4$-treated animals. Magnification bars: 1000 μm (overview), 100 μm (high magnification images of the area indicated by the square in the overview).

(K) Representative photomicrographs of liver sections (5 d after acute CCl$_4$ injury) from Alb-Cre and Alb-R3 mice stained for CD3 and counterstained with hematoxylin. Graphs indicate the percentage of CD3-positive area. Magnification bars: 1000 μm (overview), 100 μm (high magnification images of the area indicated by the square in the overview).

Bar graphs show mean ± SEM. Circles indicate Alb-Cre mice and triangles indicate Alb-R3 mice. N = 3–4 (A and B), N = 3 (C and D), N = 3–8 (E), N = 3–7 (F and G), N = 4–11 (H), N = 4–8 (I), N = 4–9 (J) and N = 4–9 (K). *p ≤ 0.05, **p ≤ 0.01, ***p ≤ 0.001 and ****p ≤ 0.0001 (t test (A-D) or (Mann-Whitney U test (E and K)).

Alb-R3 mice was also reflected by the increased number of T cells in the mutant mice at day 5 after CCl$_4$ injection; however, T cell numbers had already declined at this time point in control mice (Figure 3K). Taken together, loss of Fgfr3 in hepatocytes aggravates liver damage, pointing to a hepatoprotective function of this receptor.

Loss of Fgfr3 affects expression of metabolic, pro-fibrotic and pro-inflammatory genes in hepatocytes

To gain insight into the mechanisms underlying the cytoprotective function of Fgfr3 in hepatocytes, we first determined if activation of Stat3, a key cytoprotective transcription factor in hepatocytes (Gao, 2005), is reduced in hepatocytes of Alb-R3 *vs* Alb-Cre mice. However, the ratio of phosphorylated (activated) *vs* total Stat3 was even mildly increased in freshly isolated hepatocytes of Alb-R3 *vs* Alb-Cre mice prior to and 48 h after CCl$_4$ injection (Figures S1A and S1B). We then used an unbiased approach and searched for direct and indirect targets of Fgfr3 signaling using next generation sequencing of RNA from isolated hepatocytes 48 h following a single injection of CCl$_4$ or oil (vehicle). We used oil-injected mice instead of non-treated mice for the analysis of the non-injured liver, since this is the appropriate control for the CCl$_4$ treatment. In addition, oil treatment did not cause histological alterations of the liver, and no signs of necrosis were detected (Figure 3E). The purity of the hepatocyte fraction was verified by the absence of *Ptprc*, *Adgre1* (adhesion G protein-coupled receptor 1; F4/80) and *Vim* expression (Figures 4A−4C). A minor contamination with RNA from NPCs (in particular from immune cells) was observed in one Alb-R3 CCl$_4$-treated sample. However, it only marginally affected the overall result (see below), and we re-analyzed these data excluding this outlier in the direct comparison of CCl$_4$-treated Alb-R3 *vs* Alb-Cre mice. RNA integrity was confirmed by determination of RQN number (>8).

A single CCl$_4$ treatment strongly regulated a large panel of genes in hepatocytes (Figures 4D−4F), although expression of *Fgfr3* itself was not affected (Figure S1C). The CCl$_4$-regulated genes from mice of both genotypes cluster together (Figure 4D), indicating that the global response to CCl$_4$ injury is not affected by the *Fgfr3* knockout. As the top hit, expression of cell division cycle 20 (*Cdc20*) was more than 100-fold up-regulated in Alb-Cre and Alb-R3 mice after CCl$_4$ injection, followed by several genes encoding cyclins (e.g., cyclin B1 (*Ccnb1*)) and other cell cycle regulators (Figure 4E). This reflects the strong increase in hepatocyte proliferation in mice of both genotypes in response to CCl$_4$ injury in comparison to oil injection (Figures 3I and 3J). The top down-regulated genes encode, for example, various solute transporters and proteins involved in compound detoxification. However, expression of cytochrome P450 2E1 (*Cyp2e1*), which plays a key role in CCl$_4$ metabolization (Weber et al., 2003), was not affected by the loss of Fgfr3 (Figure S1D). These results provide important insight into the mechanisms underlying the response of hepatocytes to acute CCl$_4$ injury.

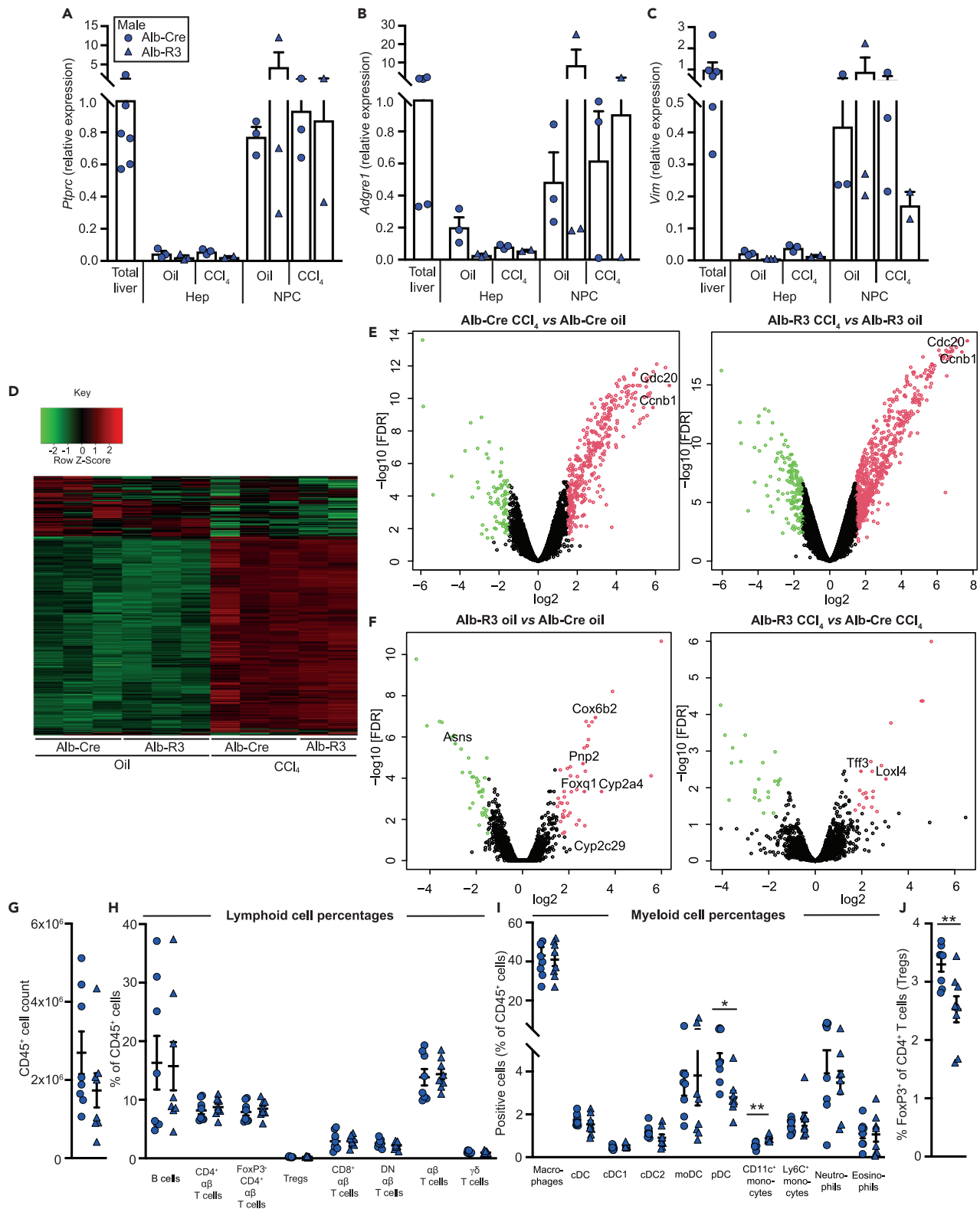**Figure 4. Loss of Fgfr3 affects the gene expression pattern in hepatocytes, but not the immune cell composition**

(A–C) qRT-PCR analysis of RNA from untreated total liver or isolated hepatocytes or NPCs from male Alb-Cre and Alb-R3 mice 48 h after injection of oil or CCl$_4$ for *Ptprc*, *Adgre1* and *Vim* relative to *Gapdh*. Hepatocyte fractions were used for RNA-seq. Expression levels in total liver were set to 1.

Figure 4. Continued

(D) Heatmap of genes with significantly different expression (FDR <0.05) in hepatocytes of Alb-R3 vs Alb-Cre mice 48 h after a single injection of CCl_4 or vehicle (oil). Genes that are significantly overexpressed or down-regulated in Alb-R3 mice are shown in red and green, respectively.

(E) Volcano plots showing genes with significantly different expression (FDR <0.05) in hepatocytes of Alb-Cre (left panel) or Alb-R3 vs Alb-Cre mice (right panel) mice, treated with CCl_4 vs oil. Genes that are significantly overexpressed in CCl_4-treated mice are shown in red, genes that are significantly down-regulated are shown in green. Genes in black are not significantly differentially expressed in the respective comparisons. Selected genes that are differentially expressed in Alb-R3 vs Alb-Cre mice after CCl_4 treatment are indicated on the respective Volcano plots.

(F) Volcano plots showing genes with significantly different expression (FDR <0.05) in hepatocytes of oil-treated (left panel) or CCl_4-treated (right panel) Alb-R3 vs Alb-Cre mice. Selected differentially expressed genes after oil or CCl_4 treatment are indicated.

(G) Number of $CD45^+$ cells in the liver of Alb-Cre and Alb-R3 mice 48 h after oil injection.

(H) Percentages of lymphoid cells among $CD45^+$ immune cells 48 h after oil injection.

(I) Percentages of myeloid cells among $CD45^+$ immune cells 48 h after oil injection.

(J) Percentage of $FoxP3^+$ cells (Tregs) among $CD4^+$ T lymphocytes 48 h after oil injection.

Bar graphs show mean ± SEM. Circles indicate Alb-Cre mice and triangles indicate Alb-R3 mice. N = 2–6 (A and B), N = 2–5 (C), N = 2–3 (D–F) and N = 8 (G–J). *$p \leq 0.05$ and **$p \leq 0.01$ (multiple t test with Holm-Sidak correction for multiple comparisons (I); unpaired t test (J)).

Relatively few genes were expressed at significantly different levels (with a false discovery rate (FDR) < 0.05) in hepatocytes from Alb-R3 vs Alb-Cre mice in the non-injured (oil-injected) liver (75 up-regulated and 133 down-regulated genes) or upon CCl_4 treatment (31 up-regulated and 30 down-regulated genes) (Figure 4F; Tables 1, 2, 3, and 4, not including "predicted genes"). Among the genes that are most strongly up-regulated in hepatocytes from oil-treated Alb-R3 vs Alb-Cre mice are genes encoding the cytochrome P450 monooxygenases Cyp2c29 and Cyp2a4, which are involved in the production of the anti-inflammatory cis-epoxyeicosatrienoic acid (Wang et al., 2020) or in hydroxylation of steroid hormones, respectively (Lavery et al., 1999). Furthermore, forkhead box Q1 (Foxq1), a transcription factor that regulates gluconeogenesis in the liver (Cui et al., 2016), was overexpressed in Fgfr3-deficient hepatocytes, suggesting alterations in glucose metabolism. This does, however, not result in major alterations in blood glucose levels or liver glycogen content under steady-state conditions (see Figures 1R–1T), although more subtle changes in glucose metabolism cannot be excluded, which may become more relevant after injury. Upregulation in Alb-R3 mice was observed for purine nucleoside phosphorylase 2 (Pnp2), which plays a key role in the purine salvage pathway, and for cytochrome c oxidase subunit 6b2 (Cox6b2), a component of the respiratory chain. Overall, these results suggest that Fgfr3 deficiency may induce widespread metabolic alterations in hepatocytes. This is further supported by the reduced expression of the gene encoding asparagine synthetase (Asns) in hepatocytes of Alb-R3 mice (Table 4).

Upon CCl_4 treatment, we found increased expression of some genes in Alb-R3 vs Alb-Cre mice, which had previously been associated with fibrotic processes (Figure 4F, right panel; Table 3). These include, for example, the genes encoding lysyl oxidase-like 4 (Loxl4), which is involved in collagen cross-linking and is overexpressed in different fibrotic tissues (Busnadiego et al., 2013; Huang et al., 2020), and trefoil factor 3 (Tff3), a small peptide hormone, which is overexpressed in kidney fibrosis (Tanaka et al., 2018) and highly abundant in the serum of patients with idiopathic pulmonary fibrosis (Doubková et al., 2016). Both proteins are secreted and may therefore affect stellate cells/fibroblasts in a paracrine manner. By contrast, several metabolic genes were downregulated, such as Cyp4a12, which is involved in fatty acid oxidation. Expression of EGFR (Egfr) and HGF receptor (Met), which are activated by major hepatocyte mitogens (EGF family members and HGF, respectively), was not affected by the loss of Fgfr3 - neither in oil-treated nor in CCl_4-treated mice (Figures S1E and S1F). This finding suggests that the enhanced liver damage in CCl_4-treated Alb-Cre mice is not a consequence of impaired expression of these receptors, but rather a direct consequence of the loss of Fgfr3 signaling. Finally, there was no evidence for impaired detoxification of reactive oxygen species in Fgfr3-deficient hepatocytes, since major targets of the cytoprotective Nrf2 transcription factor, e.g. NAD(P)H quinone dehydrogenase 1 (Nqo1), glutathione S-transferase alpha 3 (Gsta3), and glutamate-cysteine ligase catalytic subunit (Gclc) (Taguchi and Yamamoto, 2020) as well as the superoxide detoxifying enzymes superoxide dismutases 1 (Sod1) and 2 (Sod2), were normally expressed (Figures S1G–S1K).

Ingenuity Pathway Analysis (IPA) of the genes that were differentially expressed in Alb-R3 vs Alb-Cre mice following oil or CCl_4 treatment identified "Organismal Injury and Abnormalities" among the top three hits in the Diseases and Disorders category (Tables 5 and 6). The top hit in the vehicle-treated comparison was "Connective Tissue Disorders", again suggesting that genes involved in the development of fibrotic processes are already abnormally expressed under steady-state conditions. A full list of the subgroups of each of these metagroups, and genes identified in each subgroup, can be found in Tables S1 and S2.

Table 1. Top 25 up-regulated genes in RNA-Seq analysis of Alb-R3 vs Alb-Cre mice, 48 h after oil treatment

Gene	Fold differential expression	p value	FDR
Cyp2c39	46.98	1.93×10^{-7}	7.70×10^{-5}
Cyp2a4	10.64	1.69×10^{-6}	4.46×10^{-4}
Cox6b2	8.86	3.82×10^{-11}	1.14×10^{-7}
Klhl33	7.27	2.29E-10	2.88×10^{-7}
Rpgrip1	6.95	3.61×10^{-9}	2.70×10^{-6}
Ppp1r14a	6.92	3.46×10^{-9}	2.70×10^{-6}
1700028E10Rik	6.71	8.93×10^{-11}	1.78×10^{-7}
Rgs3	6.56	1.00×10^{-7}	4.61×10^{-5}
Cish	6.46	2.89×10^{-4}	2.02×10^{-2}
Foxq1	6.37	1.87×10^{-6}	4.46×10^{-4}
Poln	6.33	4.85×10^{-9}	3.41×10^{-6}
Pnp2	6.11	3.46×10^{-8}	1.97×10^{-5}
Plekhb2	5.44	1.25×10^{-4}	1.10×10^{-2}
Grm8	5.17	2.15×10^{-7}	8.31×10^{-5}
Phlda1	5.08	1.26×10^{-6}	3.59×10^{-4}
Camk2b	5.03	2.38×10^{-4}	1.79×10^{-2}
Hist1h2br	4.32	1.96×10^{-6}	4.59×10^{-4}
Erp27	4.22	1.93×10^{-7}	7.70×10^{-5}
Olfr149	4.18	5.17×10^{-8}	2.81×10^{-5}
Hist1h2bk	4.14	3.60×10^{-5}	4.81×10^{-3}
Myc	3.90	5.52×10^{-5}	6.61×10^{-3}
Tagap1	3.84	6.43×10^{-8}	3.35×10^{-5}
1700018L02Rik	3.83	8.92×10^{-6}	1.63×10^{-3}
Socs3	3.52	7.19×10^{-4}	4.16×10^{-2}
Fcgbp	3.50	3.83×10^{-6}	8.19×10^{-4}

In the basal state comparison, we also identified "Inflammatory Disease" and "Immune Cell Trafficking" among the top hits, pointing to immunological alterations already in the uninjured liver of Alb-R3 mice. To test this possibility, we performed a comprehensive flow cytometry analysis of liver immune cells 48 h after vehicle injection (Figure S2A). There was no significant difference in the total number of CD45$^+$ cells between Alb-Cre and Alb-R3 mice (Figure 4G). Lymphoid and myeloid cell percentages were also not significantly altered, with the exception of plasmacytoid dendritic cells (pDCs) and CD11c$^+$ monocytes, which were less abundant in Alb-R3 mice (Figures 4H and 4I). The total lymphoid and myeloid cell counts were comparable between genotypes (Figures S2B and S2C). The percentage of regulatory T cells (Tregs) among all CD4$^+$ T cells was significantly reduced in Alb-R3 mice; however, the percentage of Tregs in the liver was generally low, suggesting that this difference does not have a major impact (Figure 4J).

To detect potential functional differences in immune cells, NPCs were stimulated with phorbol 12-myristate 13-acetate, monensin and ionomycin, and intracellular cytokine production in various immune cell types was assessed. Stimulation panels 1 and 2 assessed levels of interferon (IFN)-γ, interleukin (IL)-10, IL-17, IL-22, and tumor necrosis factor alpha (TNF) or granulocyte-macrophage colony stimulating factor (GM-CSF), IL-4, IL-5, and IL-13, respectively. No significant difference in the expression of any of these cytokines in immune cells was observed (Figures S3A—S3J). These findings demonstrate that loss of Fgfr3 in hepatocytes has a negligible effect on immune cell composition and inflammatory state under steady-state conditions.

Loss of Fgfr3 aggravates liver fibrosis after chronic CCl$_4$ exposure

The histological and molecular alterations observed in response to a single CCl$_4$ treatment suggest that Alb-R3 mice may be primed for fibrosis because of the aggravated injury and/or the increased expression of some pro-fibrotic genes/proteins. Therefore, we subjected the animals to chronic CCl$_4$ treatment, which

Table 2. Top 25 down-regulated genes in RNA-Seq analysis of Alb-R3 vs Alb-Cre mice, 48 h after oil treatment

Gene	Fold differential expression	p value	FDR
Cebpe	−24.00	2.82×10^{-14}	1.69E-10
Acpp	−17.47	2.41E-10	2.88×10^{-7}
Lnx1	−11.95	8.57×10^{-11}	1.78×10^{-7}
H2-Bl	−11.16	1.30E-10	1.95×10^{-7}
1500015A07Rik	−7.83	7.74E-10	8.42×10^{-7}
Asns	−7.50	2.51×10^{-9}	2.14×10^{-6}
Tagap	−6.29	5.80×10^{-9}	3.85×10^{-6}
Igfbp3	−6.03	1.24×10^{-7}	5.28×10^{-5}
Nr4a1	−4.84	1.79×10^{-5}	2.86×10^{-3}
Ntrk2	−4.81	1.24×10^{-7}	5.28×10^{-5}
Ppp1r3e	−4.53	2.42×10^{-7}	8.76×10^{-5}
Lncbate6	−4.43	9.19×10^{-6}	1.64×10^{-3}
Gm20478	−3.94	2.96×10^{-7}	1.01×10^{-4}
Fam216b	−3.93	5.19×10^{-7}	1.64×10^{-4}
Olig1	−3.79	7.74×10^{-7}	2.38×10^{-4}
Sod3	−3.74	4.30×10^{-7}	1.39×10^{-4}
1700080G11Rik	−3.65	2.59×10^{-4}	1.90×10^{-2}
Ajuba	−3.53	1.73×10^{-6}	4.46×10^{-4}
Sgk1	−3.38	3.61×10^{-6}	7.84×10^{-4}
Slc15a2	−3.38	3.62×10^{-5}	4.81×10^{-3}
Xlr4b	−3.30	1.74×10^{-6}	4.46×10^{-4}
Sgce	−3.30	5.06×10^{-5}	6.18×10^{-3}
Cyp4a10	−3.28	1.24×10^{-6}	3.59×10^{-4}
Ddr1	−3.17	1.85×10^{-5}	2.90×10^{-3}
Synj2	−3.11	2.71×10^{-7}	9.54×10^{-5}

causes continuous liver injury resulting in fibrosis (Iredale, 2007). At the time of sacrifice, there was a mild, although non-significant increase in the liver-to-body weight ratio of Alb-R3 vs control mice (Figure 5A). However, Herovici and Masson Trichrome staining followed by morphometric analysis of the fibrotic area revealed much more excessive fibrosis in CCl$_4$-treated Alb-R3 vs Alb-Cre mice (Figures 5B and 5C), whereas AST and ALT serum levels were not significantly different between Alb-Cre and Alb-R3 mice (Figures 5D and 5E). The data were reproduced in an independent experiment, and the increased fibrosis was additionally confirmed by Sirius Red staining (Figures S4A−S4F). Expression of fibrosis-associated genes, including *Col1a1* and *Tgfb1*, was mildly increased in Alb-R3 mice after chronic CCl$_4$ exposure (Figures S4G and S4H). This is most likely underestimated because total liver RNA was used for this purpose. Analysis of expression levels in isolated NPCs was not possible because the extensive fibrosis prevented us from isolating pure cell populations. Interestingly, chronic CCl$_4$ treatment increased the expression of all FGF receptors in the liver. The elevation was much less pronounced in Alb-R3 mice (Figures 5F−5K). Although the reduced expression of *Fgfr3* is likely the consequence of the loss of this receptor in hepatocytes, the impaired upregulation of the other receptors may point to a role of Fgfr3 in this effect. In addition, the reduction in *Fgfr4* expression may reflect the loss of the Fgfr4-producing hepatocytes. There was a mild, but non-significant increase in Fgf9 and Fgf18 mRNA levels in the total liver of CCl$_4$-treated mice of both genotypes (Figures 5L and 5M). Taken together, these results suggest that FGFR signaling is activated after chronic liver injury in normal mice, and that a paracrine Fgf9/Fgf18-Fgfr3 signaling pathway protects hepatocytes from liver injury and fibrosis.

DISCUSSION

Ligands of the EGF and HGF receptors are key mitogens for hepatocytes with crucial functions in liver regeneration (Böhm et al., 2010a; Michalopoulos, 2007). In addition, important roles of FGFs in these

Table 3. Top 25 up-regulated genes in RNA-Seq analysis of Alb-R3 vs Alb-Cre mice, 48 h after CCl$_4$ treatment

Gene	Fold differential expression	p value	FDR
Akr1c18	9.57	6.41×10^{-8}	1.71×10^{-4}
Loxl4	8.22	8.30×10^{-6}	5.81×10^{-3}
Pnp2	7.21	2.62×10^{-6}	2.49×10^{-3}
Prom1	6.31	2.19×10^{-4}	4.48×10^{-2}
Cyp3a44	5.63	2.74×10^{-5}	1.26×10^{-2}
A2ml1	5.58	5.68×10^{-5}	1.84×10^{-2}
Klhl33	5.47	4.57×10^{-6}	3.58×10^{-3}
Hist1h2bq	5.40	1.53×10^{-4}	3.40×10^{-2}
Igsf23	5.26	1.60×10^{-6}	1.94×10^{-3}
Hist1h2bk	4.62	6.36×10^{-5}	1.92×10^{-2}
Atf3	4.61	5.86×10^{-5}	1.85×10^{-2}
Pls1	4.53	3.53×10^{-5}	1.38×10^{-2}
Scn8a	4.23	1.62×10^{-4}	3.49×10^{-2}
Nuggc	4.19	3.98×10^{-5}	1.47×10^{-2}
Tff3	3.91	4.28×10^{-6}	3.56×10^{-3}
Poln	3.77	2.49×10^{-5}	1.18×10^{-2}
Cox6b2	3.71	1.21×10^{-4}	2.92×10^{-2}
Pla2g7	3.29	1.97×10^{-4}	4.09×10^{-2}
Pglyrp1	2.80	2.55×10^{-4}	4.93×10^{-2}
Pik3c2g	2.74	7.98×10^{-5}	2.20×10^{-2}
Sprr1a	2.74	8.90×10^{-5}	2.37×10^{-2}
Abcb1b	2.64	2.59×10^{-4}	4.93×10^{-2}
Saa3	2.50	1.04×10^{-5}	6.30×10^{-3}
Abcc9	2.49	4.97×10^{-5}	1.79×10^{-2}
Wdfy1	2.46	1.17×10^{-4}	2.89×10^{-2}

processes are emerging, and we show here that cytoprotective FGF activities in the regenerating liver are mediated via Fgfr3 signaling in hepatocytes. This result complements our previous data, demonstrating that knockout of Fgfr1 and Fgfr2 alongside knock-down of Fgfr4 in hepatocytes causes liver failure after PH in most of the mice (Padrissa-Altés et al., 2015). Given that a small number of animals with Fgfr1, Fgfr2 and Fgfr4 knockout/knock-down survived after PH (Padrissa-Altés et al., 2015), we speculated that the remaining FGFR in hepatocytes – Fgfr3 – compensates at least in part for this deficiency. This hypothesis is supported by the cytoprotective function of Fgfr3 in hepatocytes, which we discovered in this study. Interestingly, expression of Fgfr3 ligands, in particular Fgf9, increased in non-parenchymal cells during liver regeneration, suggesting that a paracrine FGF-Fgfr3 signaling axis exerts beneficial effects on hepatocytes in response to acute or chronic injury. This is consistent with the identification of stellate cell-derived Fgf9 as a hepatocyte mitogen *in vitro* (Antoine et al., 2007), although we mainly observed reduced survival of Fgfr3-deficient hepatocytes, whereas their proliferation was not significantly affected. This may result from compensation by other FGF receptors. The upregulation of Fgf9 may additionally result in autocrine activation of stellate cells, which also express this receptor (Antoine et al., 2007). This could promote fibrotic processes in the liver, in particular when the cytoprotective paracrine signaling of Fgf9 via Fgfr3 in hepatocytes is abrogated as seen in Alb-R3 mice. In the future it will be important to determine if Fgfr3 signaling in hepatocytes indeed has a direct cytoprotective activity in the presence of various stressors.

The different FGF receptors in hepatocytes seem to have some overlapping, but also unique functions, depending on the type of injury. Thus, mice lacking only Fgfr1 or Fgfr2 in hepatocytes had no or only very minor abnormalities in liver regeneration (Böhm et al., 2010b), whereas mice lacking Fgfr3 showed enhanced liver necrosis, in particular in response to CCl$_4$ treatment (this study). Mice lacking both Fgfr1 and Fgfr2 in

Table 4. Top 25 down-regulated genes in RNA-Seq analysis of Alb-R3 vs Alb-Cre mice, 48 h after CCl$_4$ treatment

Gene	Fold differential expression	p value	FDR
Cebpe	−16.78	1.67×10^{-8}	5.56×10^{-5}
Lrit1	−14.76	1.83×10^{-7}	3.67×10^{-4}
Cyp4a12b	−13.03	7.39×10^{-5}	2.18×10^{-2}
Fam25c	−12.10	2.07×10^{-6}	2.11×10^{-3}
Ildr2	−11.73	4.90×10^{-7}	8.15×10^{-4}
Acpp	−9.16	1.58×10^{-6}	1.94×10^{-3}
Lnx1	−8.06	1.93×10^{-7}	3.67×10^{-4}
Lrit2	−6.11	6.13×10^{-5}	1.89×10^{-2}
Tagap	−6.00	3.22×10^{-5}	1.34×10^{-2}
Bcl7c	−5.37	9.23×10^{-6}	5.84×10^{-3}
Grid1	−5.28	7.83×10^{-5}	2.20×10^{-2}
Sall2	−4.77	1.87×10^{-6}	2.07×10^{-3}
Tlr12	−4.65	2.56×10^{-4}	4.93×10^{-2}
Adgrf1	−4.05	5.66×10^{-5}	1.84×10^{-2}
Atp10d	−4.04	2.93×10^{-5}	1.30×10^{-2}
Ppp1r3e	−3.47	2.60×10^{-4}	4.93×10^{-2}
Nox4	−3.34	1.20×10^{-5}	6.63×10^{-3}
Arl4d	−3.31	7.10×10^{-7}	1.05×10^{-3}
Tmem254b	−3.03	1.61×10^{-5}	8.22×10^{-3}
Tmem254a	−3.02	1.18×10^{-5}	6.63×10^{-3}
Nlrp12	−2.97	1.25×10^{-5}	6.63×10^{-3}
Hsd3b2	−2.85	8.81×10^{-6}	5.84×10^{-3}
Synj2	−2.39	1.31×10^{-4}	3.05×10^{-2}
9030025P20Rik	−2.23	1.15×10^{-4}	2.89×10^{-2}
Cyp2u1	−2.22	3.52×10^{-5}	1.38×10^{-2}

hepatocytes showed more severe injury after PH than *Fgfr3* knockout mice and a defect in regeneration, whereas repair after CCl$_4$ injury was not affected by the loss of Fgfr1 and Fgfr2 (Böhm et al., 2010b). Finally, mice with global Fgfr4 knockout exhibited increased liver injury and delayed repair in the CCl$_4$ injury model (Yu et al., 2002), which was similar to the phenotype observed in Alb-R3 mice. However, the effect of *Fgfr3* knockout on regeneration after PH was much milder compared to the effect of Fgfr4 knock-down in hepatocytes, which caused severe liver damage and a defect in hepatocyte proliferation after PH (Padrissa-Altés et al., 2015). Surprisingly, and in contrast to the knock-down of this receptor in adult mice, mice with global *Fgfr4* knockout did not show obvious defects in liver regeneration after PH (Yu et al., 2000), suggesting compensation by other proteins, e.g., other FGF receptors, during pre- and postnatal development. Fgfr3 is a strong candidate for such a compensatory effect, which should be tested in future studies with hepatocyte-specific knockout of both receptors. In addition, it would be of interest to assess the consequences of loss of all four FGF receptors in the context of toxic injury.

The different effects of the loss of Fgfr1, Fgfr2, Fgfr3 or Fgfr4 on liver injury and regeneration suggest that they regulate different target genes. Indeed, loss of Fgfr1 and Fgfr2 in hepatocytes caused strongly reduced expression of D-Box Binding PAR BZIP Transcription Factor (*Dbp)* and Thyrotroph Embryonic Factor (*Tef*) and their transcriptional targets, which encode cytochrome P450 enzymes involved in compound detoxification. Therefore, these mice were not able to efficiently detoxify the compounds used for anesthesia and analgesia (Böhm et al., 2010b). By contrast, expression of *Dbp* and *Tef* was not significantly affected by the loss of Fgfr3 (this study). The Fgfr4 target genes in hepatocytes of the normal and regenerating liver have not been globally analyzed yet, but signaling by this receptor suppresses the expression of genes involved in bile acid synthesis (Alvarez-Sola et al., 2018). Therefore, mice with Fgfr4 knock-down in hepatocytes or mice lacking the major Fgfr4 ligand, Fgf15, suffered from bile acid overload after PH

Table 5. Functional categories of genes identified in RNA-Seq analysis of Alb-R3 vs Alb-Cre mice, 48 h after oil treatment

'Diseases and disorders' name	p value range	# Molecules
Connective tissue disorders	1.94×10^{-3} - 8.68×10^{-9}	54
Inflammatory disease	1.70×10^{-3} - 8.68×10^{-9}	55
Organismal injury and abnormalities	2.02×10^{-3} - 8.68×10^{-9}	139
Skeletal and muscular disorders	1.59×10^{-3} - 8.68×10^{-9}	54
Cancer	2.02×10^{-3} - 1.26×10^{-7}	134
'Molecular and cellular functions' name	**p value range**	**# Molecules**
Cellular movement	2.01×10^{-3} - 4.64E-10	58
Carbohydrate metabolism	6.31×10^{-4} - 9.28×10^{-9}	30
Cell death and survival	2.01×10^{-3} - 3.16×10^{-7}	58
Cellular development	1.98×10^{-3} - 7.70×10^{-7}	62
Cellular growth and proliferation	1.83×10^{-3} - 7.70×10^{-7}	57
'Physiological system development and function' name	**p value range**	**# Molecules**
Immune cell trafficking	1.31×10^{-3} - 1.05×10^{-7}	30
Hematological system development and function	1.83×10^{-3} - 1.18×10^{-7}	46
Tissue morphology	1.98×10^{-3} - 1.18×10^{-7}	58
Cardiovascular system development and function	1.76×10^{-3} - 2.81×10^{-7}	35
Organismal development	1.76×10^{-3} - 2.81×10^{-7}	67

(Padrissa-Altés et al., 2015; Uriarte et al., 2013). Our RNA-seq data from Alb-R3 and Alb-Cre mice did not show differential expression of genes involved in bile acid synthesis, suggesting that their regulation is unique to Fgfr4. However, genes involved in other metabolic pathways were abnormally expressed in Fgfr3-deficient hepatocytes. Therefore, metabolic alterations may increase their vulnerability in response to toxin-mediated injury. Such alterations may also provide an explanation for the tail growth abnormalities of the mutant mice, which were not observed in mice lacking other FGF receptors in hepatocytes. To further determine individual and common roles of FGF receptors in hepatocytes in metabolic regulation, it will be interesting to identify differentially expressed genes in hepatocytes of mice lacking the different FGF receptors and in particular to perform a global metabolomic analysis.

Our data further show that loss of Fgfr3 signaling in hepatocytes enhances the development of fibrosis. This is most likely because of a cytoprotective effect of Fgfr3 ligands for hepatocytes as suggested by the more severe liver necrosis in Alb-R3 mice after acute injury. Aggravation of the chronic liver damage is likely to cause more severe fibrosis over time. In addition, Fgfr3 in hepatocytes may directly limit fibrosis by suppression of the expression of pro-fibrotic molecules, such as Loxl4 and Tff3, which were expressed at higher levels in hepatocytes of Alb-R3 mice. By contrast, a comprehensive flow cytometry analysis of liver immune cells did not reveal major differences between mice of both genotypes under non-challenged conditions, suggesting that the enhanced fibrosis is not a consequence of immune cell imbalances prior to injury.

Independent of the underlying mechanisms, the cytoprotective and anti-fibrotic activities of FGFR3 in hepatocytes may well have clinical implications and suggest the potential use of ligands of this receptor, for example FGF9, for the treatment of severe injury and/or prevention of fibrosis. Therefore, it will be important to determine if FGFR3 ligands are present at insufficient levels in injured and/or fibrotic human liver. Therapeutic application of Fgf9 was successful in the murine lung, where adenoviral delivery of this growth factor had an anti-fibrotic effect via Fgfr3 activation on mesothelial cells (Justet et al., 2017). However, the pro-tumorigenic activity of FGF9-mediated FGFR3 signaling in the liver should be taken into consideration (Paur et al., 2015, 2020; Seitz et al., 2020), and may require a limited duration of any FGF application. In addition, the effect of FGFR3 ligands on NPCs must be considered. Stellate cells also express this receptor (Antoine et al., 2007), and its autocrine and paracrine activation may activate a pro-fibrotic program.

Table 6. Functional categories of genes identified in RNA-Seq analysis of Alb-R3 *vs* Alb-Cre mice, 48 h after CCl$_4$ treatment

'Diseases and disorders' name	p value range	# Molecules
Cancer	2.63×10^{-2} - 2.39×10^{-4}	35
Organismal injury and abnormalities	2.63×10^{-2} - 2.39×10^{-4}	44
Reproductive system disease	2.60×10^{-2} - 2.39×10^{-4}	13
Antimicrobial response	2.53×10^{-2} - 7.61×10^{-4}	6
Inflammatory response	2.63×10^{-2} - 7.61×10^{-4}	21
'Molecular and cellular functions' name	**p value range**	**# Molecules**
Carbohydrate metabolism	2.63×10^{-2} - 3.44×10^{-5}	9
Lipid metabolism	2.16×10^{-2} - 3.44×10^{-5}	9
Small molecule biochemistry	2.63×10^{-2} - 3.44×10^{-5}	13
Drug metabolism	2.49×10^{-2} - 1.59×10^{-4}	5
Energy production	$2,16 \times 10^{-2}$ - $1,59 \times 10^{-4}$	2
'Physiological system development and function' name	**p value range**	**# Molecules**
Endocrine system development and function	2.16×10^{-2} - 1.59×10^{-4}	5
Connective tissue development and function	2.63×10^{-2} - 2.72×10^{-4}	8
Tissue morphology	2.51×10^{-2} - 2.72×10^{-4}	13
Nervous system development and function	2.46×10^{-2} - 1.36×10^{-3}	12
Cardiovascular system development and function	1.44×10^{-2} - 2.42×10^{-3}	5

This hypothesis is supported by the decreased bleomycin-induced pulmonary fibrosis in mice lacking Fgfr1, Fgfr2, and Fgfr3 in mesenchymal cells compared to control mice (Guzy et al., 2017) and the activation of a pro-fibrotic signaling pathway in systemic sclerosis in mice and humans by binding of FGF9 to FGFR3 on fibroblasts (Chakraborty et al., 2020). Therefore, the effect of Fgfr3 activation on fibrosis is likely dependent on the cell type and the tissue, and it will therefore be interesting to determine the consequences of *Fgfr3* deletion in hepatic stellate cells for the development of liver fibrosis. Such studies will be relevant for the development of strategies to activate FGFR3 signaling for the promotion of tissue repair and prevention of fibrosis.

Limitations of the study

- Our work demonstrates that signaling via Fgfr3 in hepatocytes protects from toxin-induced cell death. However, further work, e.g., *in vitro* studies with organoids, will be required to determine if this is a direct effect and to unravel the responsible signaling pathways and target genes.

- Our work further suggests that Fgfr3 signaling in hepatocytes protects from liver fibrosis. However, it is as yet unclear if this is a consequence of the hepatoprotective function and the resulting reduction in tissue damage in the presence of Fgfr3 or if Fgfr3 directly suppresses expression of secreted, pro-fibrotic molecules.

- Finally, the comparison of our results with previous data suggests individual, but also overlapping functions of different FGF receptors in hepatocytes. However, we did not directly compare the phenotype of Alb-R3 mice with the abnormalities in mice lacking other FGF receptors in hepatocytes in parallel experiments. Therefore, differences in the microbiome, the housing conditions or in the experimental procedures cannot be excluded.

STAR★METHODS

Detailed methods are provided in the online version of this paper and include the following:
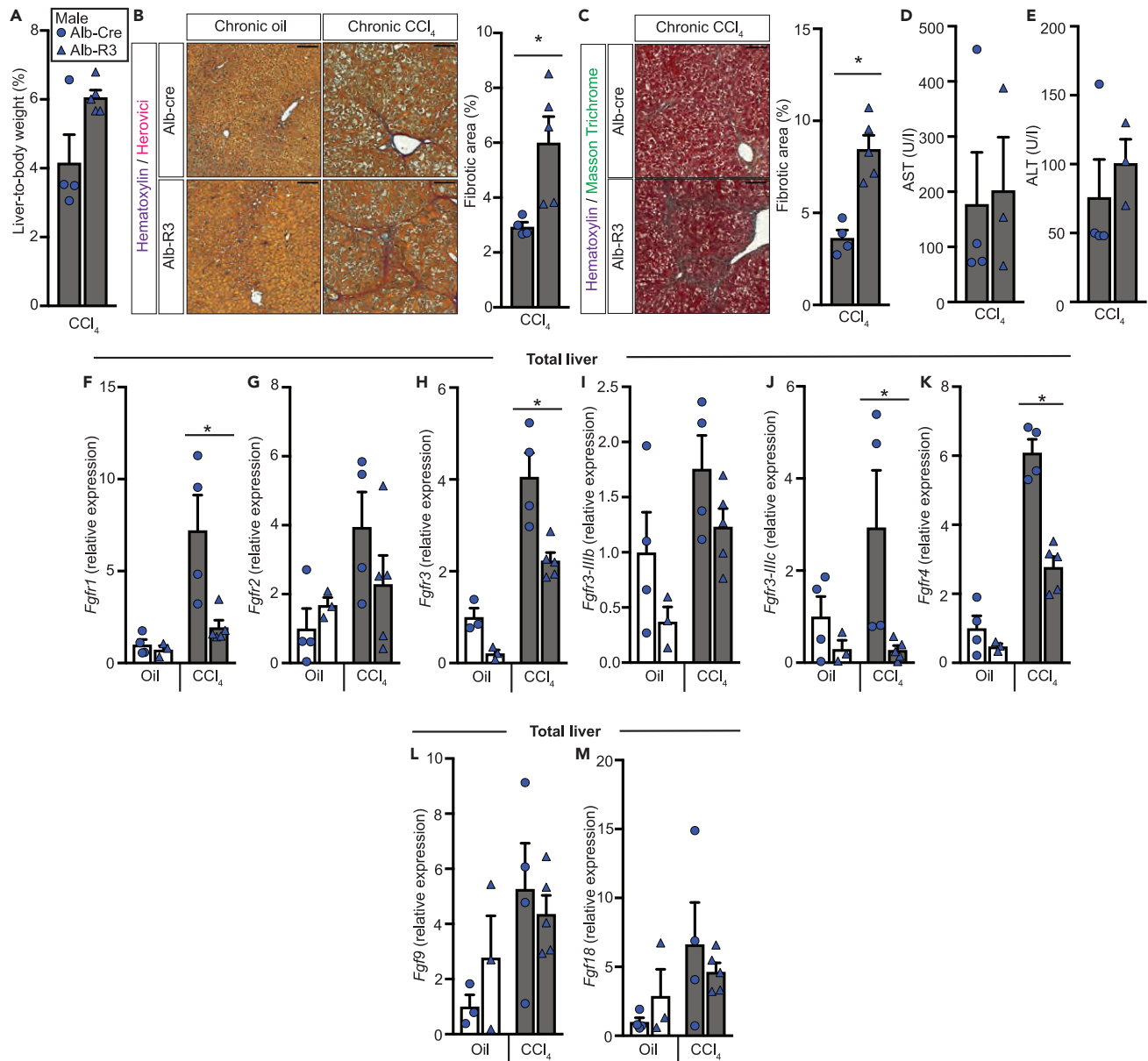
- KEY RESOURCES TABLE
- RESOURCE AVAILABILITY

Figure 5. Loss of Fgfr3 in hepatocytes aggravates fibrosis after chronic CCl$_4$ injury

(A) Liver-to-body weight ratio of male Alb-Cre and Alb-R3 mice after chronic CCl$_4$ treatment.

(B and C) Representative photomicrographs of Herovici- (B) or Masson Trichrome- (C) stained liver sections after chronic oil or CCl$_4$ treatment and quantification of the fibrotic area. Fibrotic area (identified by red/dark brown staining (B) and green/blue staining (C)) was determined by analyzing whole liver sections (20x magnification) and is shown as percentage of total liver area. Magnification bars: 100 μm.

(D and E) Serum AST and ALT levels after chronic CCl$_4$ treatment.

(F–M) qRT-PCR analysis of RNA from total liver of Alb-Cre and Alb-R3 mice after chronic CCl$_4$ treatment for *Fgfr1* (F), *Fgfr2* (G), *Fgfr3* (all variants, Fgfr3-IIIb and Fgfr3-IIIc) (H-J), *Fgfr4* (K), *Fgf9* (L) and *Fgf18* (M). Mean expression levels in oil-treated Alb-Cre mice were set to 1.

Bar graphs show mean ± SEM. Circles indicate Alb-Cre mice and triangles indicate Alb-R3 mice. N = 4–5 (A-C), N = 3–4 (D and E) and N = 3–5 (F–M). *p ≤ 0.05 (Mann-Whitney U test (B, C, F, H, J, and K)).

- ○ Lead contact
- ○ Materials availability
- ○ Data and code availability
- ● EXPERIMENTAL MODEL AND SUBJECT DETAILS

- ○ Animals
- ● METHOD DETAILS
  - ○ Partial hepatectomy (PH)
  - ○ Carbon tetrachloride (CCl_4)-induced acute liver injury
  - ○ Carbon tetrachloride (CCl_4)-induced chronic liver injury and fibrosis
  - ○ Serum collection and analysis
  - ○ Histology and histomorphometry
  - ○ Oil red O staining
  - ○ Identification of proliferating cells by BrdU labeling
  - ○ Immunohistochemistry
  - ○ Separation of hepatocytes from non-parenchymal cells (NPC)
  - ○ RNA isolation and quantitative RT-PCR (qRT–PCR) analysis
  - ○ Flow cytometry analysis of liver immune cells
  - ○ Myeloid cell panel
  - ○ Lymphoid cell panel
  - ○ NPC stimulation panel
  - ○ RNA sequencing
  - ○ Analysis of RNA-sequencing data
  - ○ Western blot analysis
  - ○ Glucose measurement
  - ○ Determination of liver glycogen content
- ● QUANTIFICATION AND STATISTICAL ANALYSIS

SUPPLEMENTAL INFORMATION

Supplemental information can be found online at https://doi.org/10.1016/j.isci.2021.103143.

AUTHOR CONTRIBUTIONS

AF: Conceptualized the study, performed experiments, analyzed data, made the figures, and wrote the manuscript together with SW.

CS: Conceptualized the study, performed experiments, and analyzed data.

AK: Performed experiments, analyzed data and made the RNA-seq figures and tables.

MB: Initiated the study, performed experiments, and analyzed data.

LT and LP: Performed and analyzed the flow cytometry data.

SP: Performed experiments, analyzed data.

TH: Performed the serological analysis.

LC: Provided mice with floxed *Fgfr3* alleles.

MK: Supervised the flow cytometry experiments.

SW: Conceptualized the study, supervised experiments, wrote the manuscript together with AF and provided the funding

All authors made important comments on the manuscript.

REFERENCES

Alvarez-Sola, G., Uriarte, I., Latasa, M.U., Jimenez, M., Barcena-Varela, M., Santamaría, E., Urtasun, R., Rodriguez-Ortigosa, C., Prieto, J., Berraondo, P., et al. (2018). Bile acids, FGF15/19 and liver regeneration: from mechanisms to clinical applications. Biochim. Biophys. Acta Mol. Basis Dis. *1864*, 1326–1334. https://doi.org/10.1016/j.bbadis.2017.06.025.

Antoine, M., Wirz, W., Tag, C.G., Gressner, A.M., Marvituna, M., Wycislo, M., Hellerbrand, C., and Kiefer, P. (2007). Expression and function of fibroblast growth factor (FGF) 9 in hepatic stellate cells and its role in toxic liver injury. Biochem. Biophys. Res. Commun. *361*, 335–341. https://doi.org/10.1016/j.bbrc.2007.06.189.

Böhm, F., Köhler, U.A., Speicher, T., and Werner, S. (2010a). Regulation of liver regeneration by growth factors and cytokines. EMBO Mol. Med. *2*, 294–305. https://doi.org/10.1002/emmm.201000085.

Böhm, F., Speicher, T., Hellerbrand, C., Dickson, C., Partanen, J.M., Ornitz, D.M., and Werner, S. (2010b). FGF receptors 1 and 2 control chemically induced injury and compound detoxification in regenerating livers of mice. Gastroenterology *139*, 1385–1396. https://doi.org/10.1053/j.gastro.2010.06.069.

Bray, N.L., Pimentel, H., Melsted, P., and Pachter, L. (2016). Near-optimal probabilistic RNA-seq quantification. Nat. Biotechnol. *34*, 525–527. https://doi.org/10.1038/nbt.3519.

Busnadiego, O., González-Santamaría, J., Lagares, D., Guinea-Viniegra, J., Pichol-Thievend, C., Muller, L., and Rodríguez-Pascual, F. (2013). LOXL4 is induced by transforming growth factor β1 through Smad and JunB/Fra2 and contributes to vascular matrix remodeling. Mol. Cell Biol *33*, 2388–2401. https://doi.org/10.1128/mcb.00036-13.

Chakraborty, D., Zhu, H., Jüngel, A., Summa, L., Li, Y.N., Matei, A.E., Zhou, X., Huang, J., Trinh-Minh, T., Chen, C.W., et al. (2020). Fibroblast growth factor receptor 3 activates a network of profibrotic signaling pathways to promote fibrosis in systemic sclerosis. Sci. Transl Med. *12*. https://doi.org/10.1126/scitranslmed.aaz5506.

Cui, Y., Qiao, A., Jiao, T., Zhang, H., Xue, Y., Zou, Y., Cui, A., Fang, F., and Chang, Y. (2016). The hepatic FOXQ1 transcription factor regulates glucose metabolism in mice. Diabetologia *59*, 2229–2239. https://doi.org/10.1007/s00125-016-4043-z.

Diehl, A.M. (2002). Liver regeneration. Front Biosci. 7, e301–314.

Doubková, M., Karpíšek, M., Mazoch, J., Skřičková, J., and Doubek, M. (2016). Prognostic significance of surfactant protein A, surfactant protein D, Clara cell protein 16, S100 protein, trefoil factor 3, and prostatic secretory protein 94 in idiopathic pulmonary fibrosis, sarcoidosis, and chronic pulmonary obstructive disease. Sarcoidosis Vasc. Diffuse Lung Dis. 33, 224–234.

Gao, B. (2005). Cytokines, STATs and liver disease. Cell Mol Immunol 2, 92–100.

Guzy, R.D., Li, L., Smith, C., Dorry, S.J., Koo, H.Y., Chen, L., and Ornitz, D.M. (2017). Pulmonary fibrosis requires cell-autonomous mesenchymal fibroblast growth factor (FGF) signaling. J. Biol. Chem. *292*, 10364–10378. https://doi.org/10.1074/jbc.M117.791764.

Halpern, K.B., Shenhav, R., Matcovitch-Natan, O., Tóth, B., Lemze, D., Golan, M., Massasa, E.E., Baydatch, S., Landen, S., Moor, A.E., et al. (2017). Single-cell spatial reconstruction reveals global division of labour in the mammalian liver. Nature *542*, 352–356. https://doi.org/10.1038/nature21065.

Huang, M., Cai, G., Baugh, L.M., Liu, Z., Smith, A., Watson, M., Popovich, D., Zhang, T., Stawski, L.S., Trojanowska, M., et al. (2020). Systemic sclerosis dermal fibroblasts induce cutaneous fibrosis through lysyl oxidase-like 4: new evidence from three-dimensional skin-like tissues. Arthritis Rheumatol. *72*, 791–801. https://doi.org/10.1002/art.41163.

Iredale, J.P. (2007). Models of liver fibrosis: exploring the dynamic nature of inflammation and repair in a solid organ. J. Clin. Invest *117*, 539–548. https://doi.org/10.1172/jci30542.

Justet, A., Joannes, A., Besnard, V., Marchal-Sommé, J., Jaillet, M., Bonniaud, P., Sallenave, J.M., Solhonne, B., Castier, Y., Mordant, P., et al. (2017). FGF9 prevents pleural fibrosis induced by intrapleural adenovirus injection in mice. Am. J. Physiol. Lung Cell Mol Physiol *313*, L781–l795. https://doi.org/10.1152/ajplung.00508.2016.

Kong, B., Huang, J., Zhu, Y., Li, G., Williams, J., Shen, S., Aleksunes, L.M., Richardson, J.R., Apte, U., Rudnick, D.A., and Guo, G.L. (2014). Fibroblast growth factor 15 deficiency impairs liver regeneration in mice. Am. J. Physiol. Gastrointest. Liver Physiol. *306*, G893–G902. https://doi.org/10.1152/ajpgi.00337.2013.

Lavery, D.J., Lopez-Molina, L., Margueron, R., Fleury-Olela, F., Conquet, F., Schibler, U., and Bonfils, C. (1999). Circadian expression of the steroid 15 alpha-hydroxylase (Cyp2a4) and coumarin 7-hydroxylase (Cyp2a5) genes in mouse liver is regulated by the PAR leucine zipper transcription factor DBP. Mol. Cell Biol *19*, 6488–6499. https://doi.org/10.1128/mcb.19.10.6488.

Lee, Y.A., Wallace, M.C., and Friedman, S.L. (2015). Pathobiology of liver fibrosis: a translational success story. Gut *64*, 830–841. https://doi.org/10.1136/gutjnl-2014-306842.

Li, C., Chen, L., Iwata, T., Kitagawa, M., Fu, X.Y., and Deng, C.X. (1999). A Lys644Glu substitution in fibroblast growth factor receptor 3 (FGFR3) causes dwarfism in mice by activation of STATs and ink4 cell cycle inhibitors. Hum. Mol. Genet. *8*, 35–44. https://doi.org/10.1093/hmg/8.1.35.

Maddaluno, L., Urwyler, C., and Werner, S. (2017). Fibroblast growth factors: key players in regeneration and tissue repair. Development *144*, 4047–4060. https://doi.org/10.1242/dev.152587.

Mehendale, H.M., Roth, R.A., Gandolfi, A.J., Klaunig, J.E., Lemasters, J.J., and Curtis, L.R. (1994). Novel mechanisms in chemically induced hepatotoxicity. Faseb j *8*, 1285–1295. https://doi.org/10.1096/fasebj.8.15.8001741.

Michalopoulos, G.K. (2007). Liver regeneration. J. Cell Physiol *213*, 286–300. https://doi.org/10.1002/jcp.21172.

Ornitz, D.M., and Itoh, N. (2015). The fibroblast growth factor signaling pathway4 (Wiley Interdiscip Rev Dev Biol), pp. 215–266. https://doi.org/10.1002/wdev.176.

Padrissa-Altés, S., Bachofner, M., Bogorad, R.L., Pohlmeier, L., Rossolini, T., Böhm, F., Liebisch, G., Hellerbrand, C., Koteliansky, V., Speicher, T., and Werner, S. (2015). Control of hepatocyte proliferation and survival by Fgf receptors is essential for liver regeneration in mice. Gut *64*, 1444–1453. https://doi.org/10.1136/gutjnl-2014-307874.

Paur, J., Nika, L., Maier, C., Moscu-Gregor, A., Kostka, J., Huber, D., Mohr, T., Heffeter, P., Schrottmaier, W.C., Kappel, S., et al. (2015). Fibroblast growth factor receptor 3 isoforms: novel therapeutic targets for hepatocellular carcinoma? Hepatology *62*, 1767–1778. https://doi.org/10.1002/hep.28023.

Paur, J., Valler, M., Sienel, R., Taxauer, K., Holzmann, K., Marian, B., Unterberger, A., Mohr, T., Berger, W., Gvozdenovich, A., et al. (2020). Interaction of FGF9 with FGFR3-IIIb/IIIc, a putative driver of growth and aggressive behaviour of hepatocellular carcinoma. Liver Int. *40*, 2279–2290. https://doi.org/10.1111/liv.14505.

Postic, C., and Magnuson, M.A. (2000). DNA excision in liver by an albumin-Cre transgene occurs progressively with age. Genesis *26*, 149–150. https://doi.org/10.1002/(sici)1526-968x.

Postic, C., Shiota, M., Niswender, K.D., Jetton, T.L., Chen, Y., Moates, J.M., Shelton, K.D., Lindner, J., Cherrington, A.D., and Magnuson, M.A. (1999). Dual roles for glucokinase in glucose homeostasis as determined by liver and pancreatic beta cell-specific gene knock-outs using Cre recombinase. J. Biol. Chem. *274*, 305–315. https://doi.org/10.1074/jbc.274.1.305.

Robinson, M.D., McCarthy, D.J., and Smyth, G.K. (2010). edgeR: a Bioconductor package for differential expression analysis of digital gene expression data. Bioinformatics *26*, 139–140. https://doi.org/10.1093/bioinformatics/btp616.

Seitz, T., Freese, K., Dietrich, P., Thasler, W.E., Bosserhoff, A., and Hellerbrand, C. (2020). Fibroblast Growth Factor 9 is expressed by activated hepatic stellate cells and promotes progression of hepatocellular carcinoma. Sci. Rep. *10*, 4546. https://doi.org/10.1038/s41598-020-61510-4.

Seitz, T., and Hellerbrand, C. (2021). Role of fibroblast growth factor signalling in hepatic fibrosis. Liver Int. https://doi.org/10.1111/liv.14863.

Serenari, M., Cescon, M., Cucchetti, A., and Pinna, A.D. (2013). Liver function impairment in liver transplantation and after extended hepatectomy. World J. Gastroenterol. *19*, 7922–7929. https://doi.org/10.3748/wjg.v19.i44.7922.

Su, N., Xu, X., Li, C., He, Q., Zhao, L., Li, C., Chen, S., Luo, F., Yi, L., Du, X., et al. (2010). Generation of Fgfr3 conditional knockout mice. Int. J. Biol. Sci. *6*, 327–332. https://doi.org/10.7150/ijbs.6.327.

Taguchi, K., and Yamamoto, M. (2020). The KEAP1-NRF2 system as a molecular target of cancer treatment. Cancers (Basel) *13*. https://doi.org/10.3390/cancers13010046.

Tanaka, K., Sugiyama, H., Yamanari, T., Mise, K., Morinaga, H., Kitagawa, M., Onishi, A., Ogawa-Akiyama, A., Tanabe, K., Eguchi, J., et al. (2018). Renal expression of trefoil factor 3 mRNA in association with tubulointerstitial fibrosis in IgA nephropathy. Nephrology (Carlton) *23*, 855–862. https://doi.org/10.1111/nep.13444.

Taub, R. (2004). Liver regeneration: from myth to mechanism. Nat. Rev. Mol. Cell Biol *5*, 836–847. https://doi.org/10.1038/nrm1489.

Trautwein, C., Friedman, S.L., Schuppan, D., and Pinzani, M. (2015). Hepatic fibrosis: Concept to treatment. J. Hepatol. *62*, S15–S24. https://doi.org/10.1016/j.jhep.2015.02.039.

Uriarte, I., Fernandez-Barrena, M.G., Monte, M.J., Latasa, M.U., Chang, H.C., Carotti, S., Vespasiani-Gentilucci, U., Morini, S., Vicente, E., Concepcion, A.R., et al. (2013). Identification of fibroblast growth factor 15 as a novel mediator of liver regeneration and its application in the prevention of post-resection liver failure in mice. Gut *62*, 899–910. https://doi.org/10.1136/gutjnl-2012-302945.

Wang, Q., Tang, Q., Zhao, L., Zhang, Q., Wu, Y., Hu, H., Liu, L., Liu, X., Zhu, Y., Guo, A., and Yang, X. (2020). Time serial transcriptome reveals Cyp2c29 as a key gene in hepatocellular carcinoma development. Cancer Biol. Med. *17*, 401–417. https://doi.org/10.20892/j.issn.2095-3941.2019.0335.

Weber, L.W., Boll, M., and Stampfl, A. (2003). Hepatotoxicity and mechanism of action of haloalkanes: carbon tetrachloride as a toxicological model. Crit. Rev. Toxicol. *33*, 105–136. https://doi.org/10.1080/713611034.

Wietecha, M.S., Pensalfini, M., Cangkrama, M., Müller, B., Jin, J., Brinckmann, J., Mazza, E., and Werner, S. (2020). Activin-mediated alterations of the fibroblast transcriptome and matrisome control the biomechanical properties of skin wounds. Nat. Commun. *11*, 2604. https://doi.org/10.1038/s41467-020-16409-z.

Williams, M.J., Clouston, A.D., and Forbes, S.J. (2014). Links between hepatic fibrosis, ductular reaction, and progenitor cell expansion. Gastroenterology *146*, 349–356. https://doi.org/10.1053/j.gastro.2013.11.034.

Yu, C., Wang, F., Jin, C., Wu, X., Chan, W.K., and McKeehan, W.L. (2002). Increased carbon tetrachloride-induced liver injury and fibrosis in FGFR4-deficient mice. Am. J. Pathol. *161*, 2003–2010. https://doi.org/10.1016/s0002-9440(10)64478-1.

Yu, C., Wang, F., Kan, M., Jin, C., Jones, R.B., Weinstein, M., Deng, C.X., and McKeehan, W.L. (2000). Elevated cholesterol metabolism and bile acid synthesis in mice lacking membrane tyrosine kinase receptor FGFR4. J. Biol. Chem. *275*, 15482–15489. https://doi.org/10.1074/jbc.275.20.15482.

Zhang, X., Ibrahimi, O.A., Olsen, S.K., Umemori, H., Mohammadi, M., and Ornitz, D.M. (2006). Receptor specificity of the fibroblast growth factor family. The complete mammalian FGF family. J. Biol. Chem. *281*, 15694–15700. https://doi.org/10.1074/jbc.M601252200.

STAR★METHODS

KEY RESOURCES TABLE

REAGENT or RESOURCE	SOURCE	IDENTIFIER
Antibodies and staining reagents		
Immunostaining:		Cat#
Anti-Ki67	Abcam, Cambridge, UK	Cat#16667
Anti-BrdU	Roche, Rotkreuz, Switzerland	Cat#11585860001
Anti-CD3	Agilent Technologies, Santa Clara, CA	Cat#A0452
Western blot		
GAPDH	HyTest, Turku, Finland	Cat#5G4
Anti-total STAT3	Cell Signaling, Danvers, MA	Cat#9131S
Anti pSTAT3 (Tyr 705)	Cell Signaling	Cat#4904S
Anti-rabbit-IgG HRP-coupled	Promega, Madison, WI	Cat#w4011
Anti-mouse-IgG HRP-coupled	Promega	Cat#w4021
Flow cytometry – Myeloid cell panel:		
Anti-XCR1	BioLegend, San Diego, CA	Cat#148208
Anti-PDCA-1	BioLegend	Cat#127007
Anti-Ly6G	BioLegend	Cat#127622
Anti-F4/80	BioLegend	Cat#123116
Anti-MHC II	BioLegend	Cat#107641
Anti-CD64	BioLegend	Cat#139309
Anti-Ly6C	BioLegend	Cat#128018
Anti-CD3	BioLegend	Cat#100348
Anti-Siglec-F	BD Biosciences, San Jose, CA	Cat#552126
Anti-CD207	Invitrogen, Carlsbad, CA	Cat#13-2075-82
Flow cytometry – Myeloid and Lymphoid cell panels:		
eFluor780	Thermo Fischer Scientific, Waltham, CA	Cat#65-0865-14
Streptavidin	BD Biosciences	Cat#563262
Anti-CD19	eBioscience, San Diego, CA	Cat#12-0193-82
Anti-NK1.1	BioLegend	Cat#12-5941-82
Flow cytometry – Myeloid, Lymphoid and NPC extracellular cell panel:		
Anti-CD11c	BioLegend	Cat#117334
Anti-CD11b	BioLegend	Cat#101257
Flow cytometry – Myeloid and NPC extracellular cell panel:		
Anti-CD45	BioLegend	Cat#103149
Flow cytometry – Lymphoid cell panel:		
Anti-FoxP3	Invitrogen	Cat#45-5773-82
Anti-CD90.2	BioLegend	Cat#105306
Anti-CD127	BioLegend	Cat#121122
Anti-CD44	BioLegend	Cat#103044
Anti-ICOS	BioLegend	Cat#313524
Flow cytometry – Lymphoid and NPC extracellular cell panel:		
Anti-TCRb	BioLegend	Cat#109224
Anti-CD45	BioLegend	Cat#103149
Anti-CD4	BioLegend	Cat#100447

(Continued on next page)

Continued

REAGENT or RESOURCE	SOURCE	IDENTIFIER
Anti-CD11b	BioLegend	Cat#101257
Anti-CD11c	BioLegend	Cat#117334
Anti-CD8a	BioLegend	Cat#100722
Anti-CD3e	BioLegend	Cat#100348
Flow cytometry – NPC stimulation panel - extracellular:		
eFluor780	Thermo Fischer Scientific	Cat#65-0865-14
Flow cytometry – Stimulation panel 1 - intracellular:		
Anti-IL-10	BioLegend	Cat#505006
Anti-IL-22	Invitrogen	Cat#17-7222-82
Anti-TNF	BioLegend	Cat#506333
Anti-IFN-γ	BD Biosciences	Cat#557649
Anti-IL-17A	Invitrogen	Cat#12-7177-81
Flow cytometry – Stimulation panel 2 - intracellular:		
Anti-GM-CSF	BioLegend	Cat#11-7331-82
Anti-IL-5	BD Biosciences	Cat#554396
Anti-IL-4	BioLegend	Cat#504118
Anti-IL-13	eBioscience	Cat#12-7133-81
Biological samples		
Mouse liver samples and sections	This study	
Critical commercial assays		
Western Bright ECL kit	Advansta, San José, CA	Cat#K-12045-D20
Glycogen-Assay-Kit	Sigma-Aldrich, St. Louis, MO	Cat#MAK016
Pierce BCA protein assay kit	Thermo Fisher	Cat#23225
Vectastain® ABC-horse radish peroxidase (HRP) Kit	Vector Laboratories, Burlingame, CA	Cat#PK4000
Deposited data		
RNA-Sequencing Data	This study	Accession number GSE176256
Experimental models: Organisms/strains		
Mice lacking Fgfr3 in hepatocytes (Alb-R3 mice) and Alb-Cre control mice	This study	
Oligonucleotides - RT-PCR primers		
Primers for Fgfr1, Fgfr2, Fgfr3, Fgfr3-IIIb, Fgf3-IIIc, Fgfr4, Fgf9, Fgf18, Col1a1, Tgfb1, Ptprc, Vimentin, Adgre1 and Gapdh see Table S3	Microsynth, Balgach, Switzerland	
Software and algorithms		
Ingenuity Pathway Analysis	Qiagen, Hilden, Germany	https://digitalinsights.qiagen.com/products-overview/discovery-insights-portfolio/analysis-and-visualization/qiagen-ipa/
ImageJ (version 1.53e)	National Institutes of Health, Bethesda, MA	https://imagej.nih.gov/ij/index.html
PRISM (version 9)	GraphPad Software Inc., San Diego, CA	https://www.graphpad.com/scientific-software/prism/
ZEN Blue (version 2.5)	Carl Zeiss, Inc., Oberkochen, Germany	https://www.zeiss.ch/mikroskopie/produkte/mikroskopsoftware/zen.html
BioRender	BioRender Inc., Toronto, ON	https://biorender.com/

RESOURCE AVAILABILITY

Lead contact

Further information and requests for resources, reagents and original data should be directed to and will be fulfilled by the lead contact Sabine Werner: sabine.werner@biol.ethz.ch.

Materials availability

This work did not generate new unique reagents.

Data and code availability

- Original RNA-seq files are deposited in the Gene Expression Omnibus and are publicly available as of the date of publication. Accession numbers are listed in the key resources table.

- This paper does not report on original codes.

- Any additional information required to re-analyze the data reported in this paper is available from the lead contact upon request.

EXPERIMENTAL MODEL AND SUBJECT DETAILS

Animals

To obtain mice lacking Fgfr3 in hepatocytes (designated Alb-R3 mice), mice with floxed *Fgfr3* alleles (Su et al., 2010) were mated with mice expressing Cre recombinase in hepatocytes (Alb-Cre mice (Postic and Magnuson, 2000) (all in C57BL/6 background). Mice were maintained under specific pathogen-free (SPF) conditions and received food and water *ad libitum*. Mouse maintenance and all procedures with animals had been approved by the local veterinary authorities of Zürich, Switzerland (Kantonales Veterinäramt Zürich), and all experiments conformed to the regulatory standards. Both male and female mice were used for the analysis, and the gender of the animals is indicated in the figure and figure legends. All experiments were performed with mice at the age of 10-12 weeks unless stated otherwise in the figure legends.

METHOD DETAILS

Partial hepatectomy (PH)

Eight- to ten-week-old male and female mice were anaesthetized by inhalation of isoflurane, and PH was performed between 8 a.m. and 12 p.m. (Padrissa-Altés et al., 2015). Mice were injected subcutaneously with buprenorphine for analgesia (Temgesic; Essex Chemie AG, Lucerne, Switzerland; 0.1mg/kg of body weight). Following euthanasia, the remaining liver was removed at different time points after PH. The liver tissue that was removed during PH was considered the 0 h time point.

Carbon tetrachloride (CCl_4)-induced acute liver injury

Eight- to ten-week-old male and female mice were injected intraperitoneally (i.p.) with a single dose of CCl_4 (0.4 mg/g body weight diluted in olive oil) or vehicle (olive oil) between 8 a.m. and 12 p.m.

Carbon tetrachloride (CCl_4)-induced chronic liver injury and fibrosis

Eight- to ten-week-old male mice were injected i.p. with CCl_4 (0.2 mg/g body weight in olive oil) or vehicle every third day over 45 days (15 injections in total). Mice were sacrificed three days after the final injection.

Serum collection and analysis

Mice were euthanized by CO_2 inhalation, and blood was taken by heart punctuation. After coagulation, serum was harvested and snap frozen. Serum ALT and AST activities were analyzed on a COBAS 8000 clinical chemistry analyzer (Roche, Rotkreuz, Switzerland).

Histology and histomorphometry

Liver samples were fixed in 4% paraformaldehyde (PFA) in PBS or in 75% ethanol/25% acetic acid and embedded in paraffin. Following deparaffination, sections (3.5 μm) were stained with hematoxylin/eosin (H&E) or using the Herovici, Masson Trichrome or Sirius Red (Abcam) staining protocols and mounted with Eukitt (Sigma, Munich, Germany) or Mowiol (Carl Roth AG, Karlsruhe, Germany). Five independent microscopic images (20x magnification) were analyzed per animal. The necrotic area was determined

morphometrically. Fibrotic area was measured in Herovici-, Masson Trichrome- and Sirius Red-stained sections (Wietecha et al., 2020).

Oil red O staining

Lipid deposits were analyzed using Oil Red O staining. Briefly, 7 μm cryosections were washed in water and 50% isopropanol and subsequently incubated for 10 min in 0.5 g Red O (Sigma), in 100 ml 60% isopropanol. Sections were then washed with 50% isopropanol, counterstained with hematoxylin, mounted with Mowiol and imaged with a Pannoramic 250 slide scanner (3D Histech, Budapest, Hungary).

Identification of proliferating cells by BrdU labeling

Mice were injected intraperitoneally (i.p.) with 5-bromo-2'-deoxyuridine (BrdU; 250 mg/kg in 0.9% NaCl; Sigma) and sacrificed 2 h after injection. Liver samples were fixed in 75% ethanol/25% acetic acid and embedded in paraffin. Sections were incubated with a peroxidase-conjugated anti-BrdU monoclonal antibody (Roche) and stained using diaminobenzidine. Sections were counterstained with hematoxylin, rehydrated and mounted using Mowiol. BrdU-positive cells were counted in 5 independent microscopic fields (20x magnification) per animal.

Immunohistochemistry

Paraffin sections were dewaxed and incubated for 30-60 min in 12% bovine serum albumin (BSA) in PBS to block unspecific binding sites. The primary antibody (anti-Ki67, Abcam, 16667; anti-CD3, Agilent Technologies-, A0452) was incubated overnight at 4°C. Sections were stained using the ABC Vectastain Peroxidase Kit (Vector Laboratories) according to the manufacturer's protocol, counterstained with hematoxylin, rehydrated, mounted, and scanned with a slide scanner (see above).

Separation of hepatocytes from non-parenchymal cells (NPC)

Mice were euthanized by CO_2 inhalation and the liver was perfused using Hanks medium (Sigma) supplemented with 0.5 mM EGTA. Mouse liver cells were isolated using digestion medium (Dulbecco's modified eagle's medium (DMEM – low glucose; Sigma) supplemented with 1% penicillin-streptomycin (P/S; Sigma) and 15 mM HEPES (Thermo Fisher Scientific). For subsequent FACS experiments, the medium was supplemented with collagenase IV (600 U/ml) and DNase 1 (200 U/ml) (both from Worthington Biochemical Corporation, Lakewood, NJ); for RNA and protein extraction, liberase TM (32 μg/ml) (Sigma) was added. Cells were then centrifuged at 50 x g for 2 min and the supernatant was collected as the NPC fraction. The cell pellet was washed with isolation medium (DMEM – low glucose supplemented with 1% P/S and 10% fetal bovine serum (FBS) (Thermo Fisher Scientific)) and centrifuged again. The supernatant was collected and added to the NPC fraction. The hepatocyte pellet was resuspended in isolation medium mix containing 40% Percoll (GE Healthcare, Chicago, IL) and centrifuged at 50 x g for 10 min. The purified hepatocytes were washed twice with isolation medium, aliquoted and processed immediately for further analyses or snap-frozen in liquid nitrogen and stored at -80°C.

The NPC fraction was centrifuged at 750 x g for 5 min. The supernatant was discarded, and the pellet resuspended in PBS supplemented with 1 mM EGTA and 2% FBS (PFB). The suspension was mixed with 40% Opti-Prep Density Gradient Medium (Sigma) and overlaid with PFB. The cells were centrifuged at 1500 x g for 25 min. The interphase was collected and washed in 10 ml isolation medium before the cells were centrifuged at 750 x g for 5 min. The cell pellet was immediately processed for further analyses or snap-frozen in liquid nitrogen and stored at -80°C.

RNA isolation and quantitative RT-PCR (qRT–PCR) analysis

Isolation of total RNA was performed using the RNeasy Mini kit (Qiagen).

RNA was reverse transcribed using the iScript™ cDNA synthesis kit (#1708890, Bio-Rad, Hercules, CA), according to the manufacturer's protocol. RT-qPCR was performed using the LightCycler®480 SYBR Green I Master reaction mix (Roche) in a LightCycler®480 II (Roche), and data were evaluated using the Light-Cycler® 480 software. Melting curve analysis was performed to exclude non-specific reactions or contaminations. All real-time samples were run in duplicates. Gene expression was determined by the $2^{-\Delta\Delta Ct}$ method. *Gapdh* was used for normalization of the expression levels of mouse genes. Primer sequences are listed in Table S3.

Flow cytometry analysis of liver immune cells

Liver cells were isolated as outlined above. The hepatocyte fraction was snap-frozen, whilst the NPC fraction was used for flow cytometry analysis. NPCs were resuspended in FACS buffer (5 mM EDTA (Sigma), 0.2% BSA in PBS) and split into three equal volumes for each immune cell panel: myeloid, lymphoid and NPC stimulation. Antibodies used for each panel are listed in the key resource table.

Myeloid cell panel

After incubating cells with an Fc receptor blocking mAb (clone 2.4G2) and extracellular staining, cells were fixed with 4% formalin and permeabilized using 0.5% saponin (Sigma). Following intracellular staining, cells were washed, resuspended in FACS buffer and the signal was acquired.

Lymphoid cell panel

After incubating cells with an Fc receptor blocking mAb (clone 2.4G2) and extracellular staining, cells were fixed and permeabilized using the Foxp3 staining kit. Following intracellular staining, cells were washed and resuspended in FACS buffer for signal acquisition.

NPC stimulation panel

NPC fractions were incubated for 3 h in Iscove's Modified Dulbecco's Medium (Thermo Fisher Scientific) supplemented with 1% P/S and 10% FBS, as well as 100 nM phorbol 12-myristate 13-acetate, 2 μM monensin and 1 μg/ml ionomycin (all from Sigma) for stimulation. They were then incubated with an Fc receptor blocking mAb (clone 2.4G2), followed by extracellular staining, fixation with 4% formalin and subsequent permeabilization using 0.5% saponin. The cell suspension was then split into two equal volumes and stained using the intracellular NPC antibody panel 1 or 2. Cells were then washed and resuspended in FACS buffer, after which signal was acquired. All cell suspensions were strained and acquired on the LSRFortessa Analyzer (BD Biosciences). Flow cytometry data were analyzed using FlowJo software, and statistical analysis was performed using Prism7 software (GraphPad Software Inc.).

RNA sequencing

Isolated primary hepatocytes were lysed in 400 μl RB buffer supplemented with 2 M dithiothreitol. RNA from these cells was isolated following the Total RNA Mini Kit (IBI Scientific, Dubuque, IO) protocol, and RNA quality was assessed using a TapeStation (Agilent Technologies, Santa Clara, CA). Samples with an RQN >8 were subjected to RNA sequencing via poly-A enrichment, True-Seq library preparation, and single-end 100 bp sequencing on a Novaseq 6000 instrument (Illumina, San Diego, CA).

Analysis of RNA-sequencing data

Alignment of reads was performed using Kallisto software, version 0.44.0 (Kallisto Software GmbH, Höxter, Germany) using the following parameters: quant -t 8 –bias –bootstrap-samples 10 –seed 42 –single –rf-stranded –fragment-length 150 –sd 70, and reference genome version GRCm38.p6 from the GENCODE project with gene model annotation version M23. For differential expression analysis, the edgeR software, version v3.28.0 (Bray et al., 2016; Robinson et al., 2010) was used with the following parameters: Normalization method – TMM (trimmed mean of m-values), data modelling – glm (generalized linear model), statistical test – QL (quasi likelihood), Benjamini Hochberg (BH) multiple testing correction. Prior to differential expression analysis, data were filtered by estimated counts with the threshold of 20 to avoid inclusion of genes that are expressed at extremely low levels.

Pathway analysis was performed based on the significantly regulated genes (false discovery rate (FDR) < 0.05 and a |log2 fold change| >=1) using Ingenuity Pathway Analysis (IPA) software, Version 26127183 (Qiagen) and the built-in right-tailed Fisher Exact Test with BH multiple testing correction.

Western blot analysis

Primary hepatocytes were isolated as outlined above. Protein was extracted using T-per buffer (ThermoFisher Scientific) supplemented with cOmplete™ protease inhibitor cocktail (Roche) and phosphatase inhibitors (PhosSTOP™, Roche). Protein concentrations were determined using a BCA Protein Assay Kit (Pierce Biotechnology, Waltham, MA). 20 μg protein was separated on a 10% polyacrylamide gel, followed by transfer onto a PVDF membrane. After blocking in 5% BSA, membranes were incubated overnight at 4°C with either anti P-Tyr705-STAT3 (9131S, Cell Signaling, 1:1000) or anti total STAT3

(4904S, Cell Signaling, 1:2000) primary antibodies, both diluted in 5% BSA. GAPDH (detected with antibody 5G4, HyTest, 1:20000) was used as a loading control. After 1 h of incubation at room temperature with anti-rabbit-IgG (w4011, Promega, 1:5000 in 5%BSA) or anti-mouse-IgG (w4021, Promega, 1:5000 in 5% BSA); both coupled to horseradish peroxidase, membranes were washed and bands were visualized using the Westernbright chemoluminescence detection kit (Advansta, San Jose, CA).

Glucose measurement

Blood glucose levels were measured post-starvation (6 h during the night) of the mice using a glucometer (Contour NEXT, Parsippany-Troy Hills, NJ).

Determination of liver glycogen content

Glycogen content of the liver was determined in the morning in mice, which had received food and water *ad libitum*, using a glycogen assay kit (MAK016, Sigma). Briefly, snap-frozen liver tissue was homogenized in ultra-pure water (100 μl for 10 mg tissue), boiled for 5 min at 95°C and centrifuged at 13'000 x g for 5 min. The supernatants were transferred to a new tube and kept on ice until ready for measurement. The assay was conducted in a transparent, flat-bottomed 96-well plate, and colorimetric absorbance was measured with a GloMax® Discover System (Promega).

QUANTIFICATION AND STATISTICAL ANALYSIS

Statistical analysis of the FACS data and RNA sequencing data is described above. Statistical analysis of all other data was performed using the Prism9 software (GraphPad Software Inc.). Quantitative data are expressed as mean $\pm$ SEM. Significance was calculated using the Mann–Whitney U test or a t-test as specified in the figure legends. *P $\leq$0.05, **P $\leq$0.01, ***P $\leq$0.001 and ****P $\leq$0.0001. All statistical details for experiments can be found in the figure legends.